



저작자표시-비영리-동일조건변경허락 2.0 대한민국

이용자는 아래의 조건을 따르는 경우에 한하여 자유롭게

- 이 저작물을 복제, 배포, 전송, 전시, 공연 및 방송할 수 있습니다.
- 이차적 저작물을 작성할 수 있습니다.

다음과 같은 조건을 따라야 합니다:



저작자표시. 귀하는 원저작자를 표시하여야 합니다.



비영리. 귀하는 이 저작물을 영리 목적으로 이용할 수 없습니다.



동일조건변경허락. 귀하가 이 저작물을 개작, 변형 또는 가공했을 경우에는, 이 저작물과 동일한 이용허락조건하에서만 배포할 수 있습니다.

- 귀하는, 이 저작물의 재이용이나 배포의 경우, 이 저작물에 적용된 이용허락조건을 명확하게 나타내어야 합니다.
- 저작권자로부터 별도의 허가를 받으면 이러한 조건들은 적용되지 않습니다.

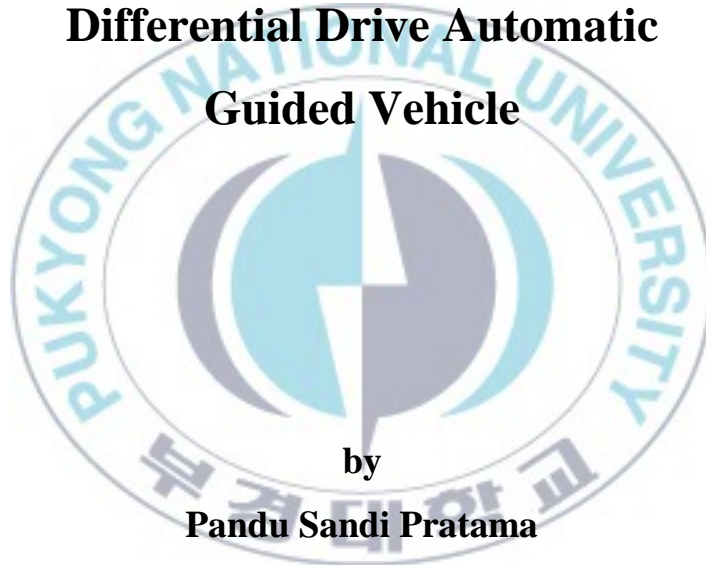
저작권법에 따른 이용자의 권리는 위의 내용에 의하여 영향을 받지 않습니다.

이것은 [이용허락규약\(Legal Code\)](#)을 이해하기 쉽게 요약한 것입니다.

[Disclaimer](#)

**Thesis for the Degree of Master of Engineering**

**Obstacle Avoidance Algorithm Based on  
Velocity and Orientation Controls of  
Differential Drive Automatic  
Guided Vehicle**



**by**

**Pandu Sandi Pratama**

**Department of Interdisciplinary Program of  
Mechatronics Engineering, The Graduate School,  
Pukyong National University**

**February 2013**

**Obstacle Avoidance Algorithm Based on  
Velocity and Orientation Controls of  
Differential Drive Automatic  
Guided Vehicle**

차동 무인 운송차량의 속도 및 방향제어에  
기초한 장애물 회피 알고리즘

by

**Pandu Sandi Pratama**

**Advisor: Professor Sang Bong Kim**

A thesis Submitted in Partial Fulfillment of the Requirements  
for the Degree of

**Master of Engineering**

**To the Department of Interdisciplinary Program of  
Mechatronics Engineering, The Graduate School,  
Pukyong National University**

**February 2013**

# Obstacle Avoidance Algorithm Based on Velocity and Orientation Controls of Differential Drive Automatic Guided Vehicle

A thesis

By

**Pandu Sandi Pratama**

Approved as to styles and contents by:

**Yeon Wook Choe**

Chairman

**Young Seok Jung**

Member

**Sang Bong Kim**

Member

February 2013

## Acknowledgements

First of all, I would like to humble myself toward Allah SWT, the Loving and Merciful Lord, because of His grace and help, I can carry on my study in here properly.

I would like to express the most gratitude to my supervisor, Professor Sang Bong Kim, for his valuable advice, guidance and support during the process of my studying in Korea. He has been providing a large amount of knowledge, the direction and skill of research, and strong motivation for my researching. His kindness, insight and continuous supports encouraged and helped me to accomplish my research and finish this dissertation scientifically.

I would like to thank the members of my thesis committee, Prof. Yeon Wook Choe and Prof. Young Seok Jung, for their helpful comments and suggestions for my thesis.

I would like to thank Prof. Hak Kyeong Kim for his great helps to research and complete this thesis. I could not finish my dissertation on time without his great help.

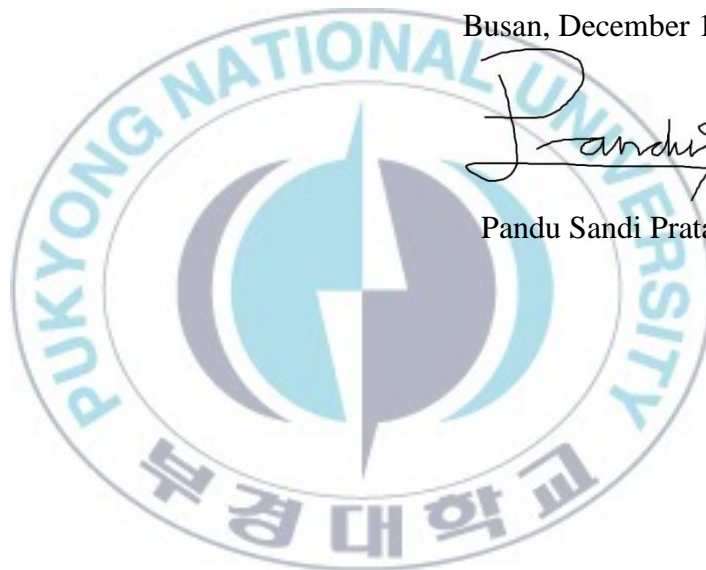
I would like to thank all members of Computer Integrated Manufacturing Electronics Commerce (CIMEC) laboratory for their cooperation and for all the kindness and friendship, Mr. Seo Kwang Kim, Mr. Viet Tuan Dinh, Mr. Jeong Geun Kim, Mr. Phuc Think Doan, Mr. Bui Thanh Luan, Mr. Hoang Giang, Miss. Yu Mi Park, Miss. Min Ji Bae, Mr. Woo Yeung Jung, Mr. Chetanraj D. Patil, Mr. Waleed M.A. Elhalwagy, Mr. Jin Uk Kim, Mr. Hyo Jun Im, for all scientific discussions and helps.

Finally, I would like to thank to my father, Sutiyoso, S.T., my mother, Ngesti Handayani Lestari, my brother, Satria Yudha Pratama, and all my close relatives for their love, endless pray, encouragement and support for me not only in the dissertation time but also in the whole of my life. Thank you to all of Indonesian student who lived in Busan. And lastly, thank you to all the people who cannot be mention here for the help and support.

Busan, December 14, 2012



Pandu Sandi Pratama



# Contents

## Acknowledgements

<b>Contents</b> .....	<b>i</b>
<b>ABSTRACT</b> .....	<b>iii</b>
<b>List of Figure</b> .....	<b>v</b>
<b>List of Tables</b> .....	<b>viii</b>
<b>Chapter 1: Introduction</b> .....	<b>1</b>
1.1. Background and Motivation.....	1
1.2. Previous Study.....	4
1.3. Objective and Research Method .....	8
1.4. Outline of thesis and contribution .....	9
<b>Chapter 2: System Description</b> .....	<b>11</b>
2.1. Mechanical Design.....	11
2.2. Electrical Design .....	14
2.2.1. Sensors.....	15
2.2.2. Controller.....	23
2.2.3. Actuator .....	25
2.2.4. Power supply .....	26
2.3. Software development.....	28
<b>Chapter 3: System Modeling</b> .....	<b>31</b>
3.1. Characterization of wheels.....	33
3.1.1. Fixed standard wheel for driving wheel .....	33
3.1.2. Castor wheel .....	34
3.2. Kinematic modeling of differential drive AGV system.....	35
3.3. BLDC motor modeling.....	41
3.4. Velocity and orientation controller design.....	48
3.5. Full structure of AGV control algorithm for velocity and orientation control.....	53

<b>Chapter 4: Obstacle Avoidance Algorithm.....</b>	<b>54</b>
4.1. Obstacle Detector .....	54
4.2. Moving Object Tracking Based on Kalman Filter .....	56
4.3. Collision Possibility Prediction .....	58
4.4. Obstacle Avoidance Policy .....	60
<b>Chapter 5: Simulation and Experimental Results.....</b>	<b>62</b>
5.1. Simulation result .....	64
5.1.1. Velocity and orientation controller.....	64
5.1.2. Obstacle avoidance algorithm .....	70
5.2. Experimental Results.....	73
5.2.1. Velocity and orientation controller.....	73
5.2.2. Obstacle avoidance algorithm .....	76
<b>Chapter 6: Conclusions.....</b>	<b>80</b>
6.1. Conclusion.....	80
6.2. Future works.....	82
<b>References.....</b>	<b>84</b>
<b>Publications and Conferences.....</b>	<b>91</b>
<b>Apendix A .....</b>	<b>93</b>

**Obstacle Avoidance Algorithm Based on Velocity and  
Orientation Control for Differential Drive  
Automatic Guided Vehicle**

Pandu Sandi Pratama

Department of Interdisciplinary Program  
of Mechatronics Engineering,  
Graduate School, Pukyong National University

**ABSTRACT**

Automatic Guided Vehicles (AGV) is common equipment to transport the materials in production process. To guarantee the safety of workers while the AGV moves around inside the factory, the moving object tracking and avoiding algorithm should be applied on the AGV.

This thesis proposes an obstacle avoiding algorithm based on velocity and orientation controller for differential drive Automatic Guided Vehicles (AGV) system to avoid the stationary and moving obstacle in industrial environment. This algorithm can works in unknown environment, and guarantees the reachability condition of goal point. To do this task, the followings are done. Firstly, the system configuration of AGV is described. A real AGV system is developed with several interconnected devices such as industrial PC as main controller, laser measurement system for obstacle detection, laser navigation system for positioning, motors for actuator and

batteries for power supply. Secondly, mathematic modeling of the AGV is presented to understand its characteristic and behavior. A velocity and orientation control is proposed based on optimal control method. The objective of the controller is to make the AGV navigate to the desired direction decided by avoidance algorithm with profiled velocity. Thirdly, the obstacle avoidance algorithm is proposed. This algorithm has several abilities such as: to detect the moving objects, to predict the velocity and direction of moving objects, to predict the collision possibility and to plan the avoidance maneuver. For sensing the local environment and positioning, the laser measurement system LMS-151 and laser navigation system NAV-200 are applied. Based on the measurement results of the sensors, the stationary and moving obstacles are detected and the collision possibility is calculated. The velocity and direction of the obstacle are predicted using Kalman filter algorithm. Collision possibility, time, and position can be calculated by comparing the AGV movement and obstacle prediction result obtained by Kalman filter. Finally, the avoidance maneuver using the well known tangent Bug algorithm is decided based on the calculation data. Finally, the effectiveness of the proposed algorithm is verified using simulation and experiment. Several examples of experiment conditions are presented using stationary obstacle, and moving obstacles. The simulation and experiment results show that the AGV can detect and avoid the obstacles successfully in all experimental condition.

**Keywords:** AGV, velocity and orientation control, obstacle avoidance.

## List of Figure

Fig. 1.1 Applications of automatic guided vehicle .....	2
Fig. 1.2 AGV's Navigation method.....	5
Fig. 2.1 AGV system used for the thesis. ....	11
Fig. 2.2 System configuration.....	12
Fig. 2.3 Configuration of differential drive AGV system.....	13
Fig. 2.4 Hardware configuration of AGV .....	14
Fig. 2.5 Laser measurement system basic principle .....	16
Fig. 2.6 Scanning area of LMS-151.....	17
Fig. 2.7 Laser Measurement System LMS-151 .....	18
Fig. 2.8 Position measurement of the NAV-200.....	19
Fig. 2.9 Laser navigation system NAV-200 .....	21
Fig. 2.10 Industrial PC TANK-800.....	23
Fig. 2.11 Motor driver.....	25
Fig. 2.12 BLDC motor .....	25
Fig. 2.13 Structure of Battery .....	27
Fig. 2.14 Flowchart program of the AGV.....	28
Fig. 2.15 Flowchart of obstacle avoidance algorithm.....	29
Fig. 2.16 Interface of AGV program .....	29
Fig. 3.1 Coordinate of AGV's modeling .....	31
Fig. 3.2 A fixed standard wheel and its parameters .....	33
Fig. 3.3 A castor wheel and its parameters .....	35
Fig. 3.4 Coordinate of differential drive AGV system .....	36
Fig. 3.5 Definition of error in proposed AGV system .....	40
Fig. 3.6 A typical BLDC motor system arrangement .....	42
Fig. 3.7 Block diagram of the control system.....	53

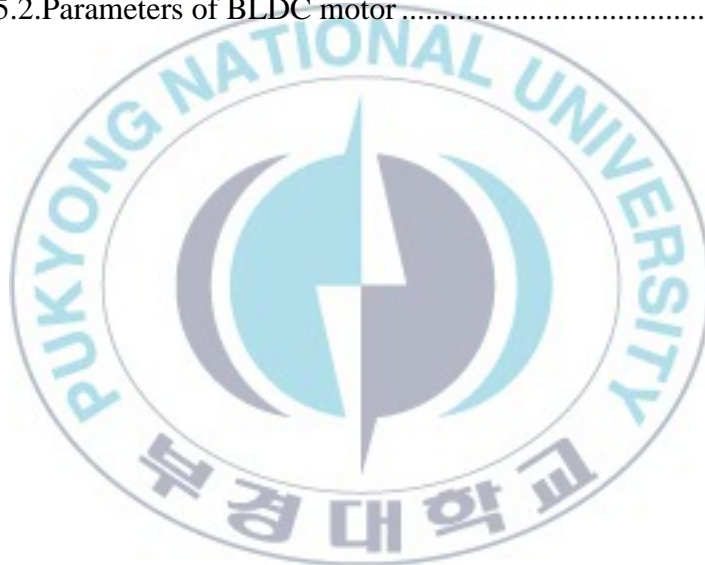
Fig. 4.1 LMS-151 scanning area.....	54
Fig. 4.2 Positioning using NAV-200 .....	55
Fig. 4.3 Obstacle projection .....	59
Fig. 4.4 Tangent Bug algorithm.....	61
Fig. 5.1 Dimension of AGV.....	62
Fig. 5.2 Control input voltages for left and right wheels .....	67
Fig. 5.3 Output of linear velocity.....	68
Fig. 5.4 Output of orientation .....	69
Fig. 5.5 Linear velocity error .....	69
Fig. 5.6 Orientation error .....	70
Fig. 5.7 Simulation environment .....	70
Fig. 5.8 Simulation results for stationary obstacle.....	71
Fig. 5.9 Simulation results for moving obstacle with transversal direction .....	72
Fig. 5.10 Simulation results for moving obstacle with longitudinal direction .....	73
Fig. 5.11 Control input voltages for left and right wheels.....	74
Fig. 5.12 Linear velocity of AGV.....	74
Fig. 5.13 Orientation of AGV.....	75
Fig. 5.14 Linear velocity error.....	75
Fig. 5.15 Orientation error .....	76
Fig. 5.16 Stationary obstacle avoidance .....	77
Fig. 5.17 Simulation and experiment trajectories for stationary obstacle avoidance.....	77
Fig. 5.18 Moving obstacle avoidance in transversal direction .....	78
Fig. 5.19 Simulation and experiment trajectories for moving obstacle in transversal direction .....	78
Fig. 5.20 Moving obstacle avoidance in longitudinal direction .....	79

Fig. 5.21 Simulation and experiment trajectories for moving  
obstacle in longitudinal direction .....79



## List of Tables

Table 2.1 Specification of laser measurement system LMS-151 .....	18
Table 2.2 Specification of Laser navigation system NAV-200 .....	22
Table 2.3 Specification of PC TANK-800.....	24
Table 2.4 Specification of BLDC motor SWIS BG90-S024 .....	26
Table 2.5 Battery Rocket AGM 80-12 parameters .....	27
Table 5.1 Parameter of AGV .....	63
Table 5.2.Parameters of BLDC motor .....	63



# Chapter 1: Introduction

## 1.1. Background and Motivation

Automatic Guided Vehicle (AGV) is defined as a materials handling system that uses independently operated, self-propelled vehicles that are guided along defined pathways in the floor [1]. The AGV can carry carts, pallet or trays and move between different manufacturing and warehouse stations without driver. These systems are used to increase efficiency and decrease the damage of goods by limiting the number of employees required to complete the job.

There are many applications of AGV in many engineering fields such as shown in Fig. 1.1. The first AGV invented by Berrett Electronics in 1953 [2] was designed for factory environment as shown in Fig. 1.1(a). It can tow objects behind them autonomously to move raw materials or finished product. Since that, the industrial AGV such as CeMAT 2005 [3] and OMG 808 FS [4] were developed and used for transporting the material from one manufacturing station to another manufacturing station. The AGV technology then is adapted in the hospital environment as shown in Fig. 1.1(b). Helpmate was one of the pioneer implementations of automated robotic hospital transportation systems [5]. It was designed for transporting small cargo between departments, and it was able to autonomously navigate inside the hospitals and take elevators. Care-o-bot was developed to provide physical support to people requiring mobility, remote inspection, and navigation capabilities [6]. I-Merc was introduced in [7] as a new and automated method of distributing

meals in hospitals. In [8], a system that consists of mobile robots and automated pick-up/delivery stations is introduced. In agriculture environment as shown in Fig. 1.1(c), the AGV technology was also adapted. In [9], an AGV for precision spraying and precision fertilization have been developed. In [10], the AGV help the farmer to harvest the apples. In [11], the AGV was able to harvest the grain, mow the grass, and plant the seed. In harbor environment as shown in Fig. 1.1(d), the AGV is used for transporting the container from the ship to storage yard and vice versa [12]. AGVs were first used for transporting containers in 1993 at the Delta/Sea-Land terminal located in Rotterdam. The AGV system was also applied to two other large European terminals, Euromax in Rotterdam and Altenwerder in Hamburg.



(a) Factory Environment



(b) Hospital Environment



(c) Agriculture environment



(d) Harbor environment

Fig. 1.1 Applications of automatic guided vehicle

To guarantee the safety of workers while the AGV moves around inside the factory, the obstacle collision avoidance must be achieved. In the past, obstacle detection systems largely consisted of mechanical bumpers and giant emergency stop button that stop the AGV in front of a person or obstacle. In particular, if the velocity of the AGV is high when the obstacle is detected, the AGV don't have enough time to brake safely due to the momentum of AGV. A proposed change to the American Society of Mechanical Engineers (ASME) B56.5 standard [13] allows non-contact safety sensors as opposed to contact sensors such as bumpers on AGVs. By replacing the contact sensor with non-contact safety sensors, vehicles can be shorter in length, excluding mechanical bumpers, allowing shorter turning radii and potentially move faster as objects can be detected well before the vehicle is close to an object [14]. Non-contact safety sensors such as infrared distance sensor, ultrasonic sensor, camera sensor and laser measurement system can be applied in AGV system. By measuring the distance between AGV and obstacle using the non-contact safety sensors, the location of obstacle can be determined. This location is then compared with the safety and warning zones predefined in the device. If the person or object is present inside the warning zone, audible and visible signals can be triggered. If intrusion of the safety zone occurs, the sensor sends a stop signal to the AGV controller. In real application, when the obstacle is detected in front of AGV, the AGV only stops and waits until the obstacle disappears. To increase the safety and time efficiency of AGV, the obstacle avoidance algorithm is needed. To avoid the collision condition, the AGV should detect the moving object in time and make reasonable decision to avoid the obstacle.

## 1.2. Previous Study

For obstacle avoidance algorithm of AGV, navigation system and obstacle detection is important for AGV to move between start and goal position and detect the obstacle.

There are several kinds of AGV navigation methods. L. Armesto [15], C. R. Kelber [16] and P. T. Doan [17] proposed a vision based line tracking algorithm as shown in Fig. 1.2(a). The AGV follows a visual line painted or embedded in the floor using camera sensor. C. Chen [18] proposed an inductive guidance using electrical wire buried under the floor as shown in Fig. 1.2(b). The wire transmits different frequency signals of about 3 - 10 Khz, then the system detects signals via coil sensors mounted in AGV. Those navigation systems are not flexible since the path can't be changed easily. T. Fujimoto [19] and S.Y. Lee [20] proposed semi-guided navigation methodology by using magnetic tapes as shown in Fig. 1.2(c). The magnetic tapes are only placed at the start and the goal points and it is used as reference to recalibrate the real position of AGV. S. C. Yuan [21] proposed the navigation method based on wall following algorithm as shown in Fig. 1.2(d). This navigation method is flexible and simple because it doesn't need to install the given path on the floor. On the other hand, the application of this method in open space such as in factory is difficult. The most advanced positioning system for indoor application is laser navigation system such as in [22-25] as shown in Fig. 1.2(e). The laser navigation system's scanner emits an invisible light impulse and measures the time to receive the reflections from reflectors. It is flexible because it doesn't need the given path on the floor and suitable for factory environment.

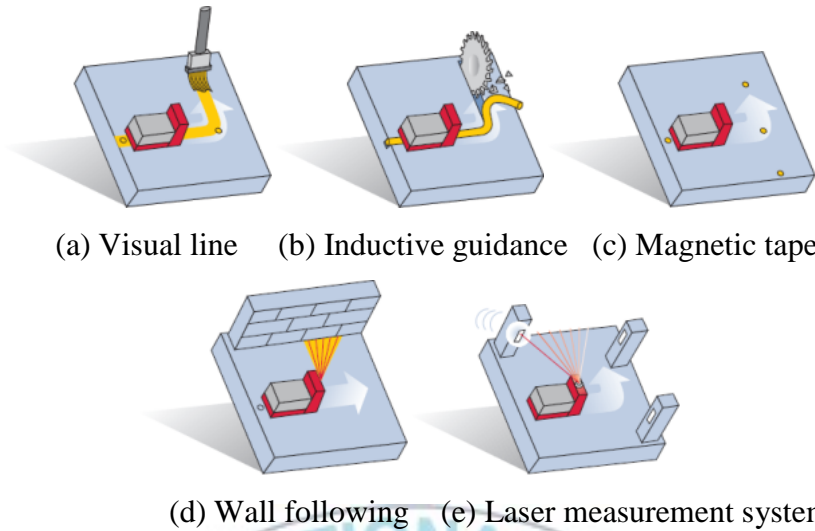


Fig. 1.2 AGV's Navigation method

In navigation algorithm, the main problem is to develop a good velocity and orientation control algorithm. The control algorithm design depends on the AGV wheel configuration. R. Siegwart [39] classified the wheel configuration in 17 types based on the number and the type of wheels. Among those wheel configurations, differential drive configuration is most widely used for industrial AGV. The navigation control algorithm generally only considers trajectory tracking. The AGV only follow the given path using visual line, inductive guidance, magnetic tape or wall. T. Y. Abdalla [41] proposed PID controller for trajectory tracking, but didn't guarantee stability for nonholonomic system. P. T. Doan [17] proposed fuzzy-PID to control the navigation of AGV, but it didn't consider the system uncertainties and external disturbance. Therefore, A. Filipescu [42] proposed trajectory tracking based on sliding mode control theory. However, trajectory tracking based control algorithm such in [17, 41, 42] are not suitable for obstacle avoidance due to the fixed

trajectory. The laser sensor technology allows the AGV to navigate around the environment without fixed path. F. Pourboghrat [43] proposed point to point navigation algorithm based on Lyapunov stability technique. However, in this algorithm, the velocity profile is exponential. In the real application, the AGV should navigate smoothly with constant velocity. Therefore, AGV navigation control method based on the velocity control using profiled velocity is needed.

For obstacle detection, the sensor for detecting the obstacle is needed. P. M. Vaz [26] proposed infrared distance sensor for obstacle avoidance and docking. A pulse of light is emitted and then reflected back. When the light returns, it comes back at an angle that is dependent on the distance of the reflecting object. The infrared sensor reading will be different for different surfaces, different colors and different shades even if the range is the same. R. Tong [27] proposed ultrasonic range finder for docking system. M. Yahyei [31] and J. Borenstein [38] proposed ultrasonic based obstacle avoidance algorithm. Ultrasonic sensors use sound instead of light, so it can be used outside in bright sunlight. However, the ultrasonic sensor doesn't work for sound absorber material such as sponge. R. V. Bostelman [28] and M. Seelinger [30] proposed an obstacle detection using camera sensor. Spampinato [29] proposed stereo vision using camera sensor for localization and obstacle detector. The obstacle can be detected using stereo camera based on triangulation method. The camera detection result depends on the lighting quality. N. Kimura [32] proposed laser measurement system to detect other robots and obstacles. The laser measurement system is an electro-optical laser measurement system that scans the perimeter of its surroundings in a

plane with the aid of laser beams. The laser measurement system measures its surroundings in two-dimensional polar coordinates. If a laser beam is incident on an object, the position is determined in the form of distance and direction.

In the real environment, the obstacle consists of stationary obstacle and moving obstacle. A. K. Tran [45] proposed a stationary obstacle avoidance using ceiling-mounted camera based on Hamilton-jacobi- Bellman equation. H. Giang [46] proposed obstacle avoidance using A\* algorithm. Those algorithms only focus in stationary obstacle algorithm and path planning. However, in real factory environment, the obstacles consist of stationary obstacle and moving obstacle. For moving obstacle avoidance algorithm, there are two ways to deal with moving object in the obstacle avoiding process. The first one does not consider the motion of object, but improve the motion planning ability and responding ability of AGV such as Artificial Potential Field [34] and grid algorithm [35]. J. G. Kim [43] proposed navigation and obstacle avoidance algorithm using D\* algorithm. Those kinds of algorithms need computation time to replan the trajectory and only work in known environment. The second one is to forecast the relative motion of object to AGV, and then adapt reasonable avoiding policy according to the anticipated collision time and position such as in [36-37], which is more effective for quick motion of AGV and the object. Those algorithms don't consider the path planning but only track the given path and not guarantee the reachability condition of goal point. Therefore, a new obstacle avoidance algorithm for stationary and moving obstacle that can works in unknown environment, and guarantee the reachability of goal position is needed.

### **1.3. Objective and Research Method**

From the above discussions, the objective of this thesis is to propose an obstacle avoidance algorithm based on velocity and orientation controller for differential drive Automatic Guided Vehicles (AGV) system to avoid the stationary and moving obstacle in industrial environment. This algorithm can work in unknown environment, and guarantee the reachability condition of goal point. To do those tasks, the followings are done. Firstly, the differential drive AGV modeling is derived with physics and mathematical derivations. Kinematic equations for AGV and BLDC motor are derived to design the velocity and orientation control navigation. This mathematical modeling is used in simulation and controller design. Secondly, velocity control and position control are proposed for navigation with velocity profiled. The controller is designed based on the optimal control theory. This control method guarantees the AGV tracking the given reference velocity and orientation. Thirdly, the obstacle avoidance algorithm is proposed to avoid stationary and moving obstacle. The object tracking algorithm based on the laser measurement result estimates the current state and future state of moving obstacle using Kalman filter algorithm. The data process and responding speed are quick. For obstacle avoiding policy, the tangent Bug algorithm is proposed to avoid the obstacles and find the shortest path from current position to the goal position. Finally, to verify the effectiveness of proposed velocity and orientation controllers and obstacle avoidance algorithm, the simulation and experiment are done. Experiments are presented using stationary obstacle and moving obstacles.

## **1.4. Outline of thesis and contribution**

### **Chapter 1: Introduction**

In this chapter, background and motivation of the thesis is described. Objective and research method of this thesis are presented. Finally, the outline of content and summary of contribution of this thesis is given.

### **Chapter 2: System description**

The hardware structure of AGV is described briefly in this chapter. This chapter consists of the hardware configuration including industrial PC, laser measurement system, laser positioning system, motors and batteries.

### **Chapter 3: System modeling**

This chapter proposes the mathematical modeling of differential drive AGV. Kinematic modeling of differential drive system and BLDC motor are presented. The velocity and orientation controllers based on optimal control method are proposed to navigate from start to goal point.

### **Chapter 4: Obstacle avoidance algorithm**

This chapter focuses on the obstacle avoidance algorithm that needs to prevent the collision condition of AGV. This algorithm consists of obstacle detection based on laser measurement system and laser positioning system, moving object prediction by Kalman filter, collision possibility prediction, and obstacle avoidance maneuver using bug algorithm.

## **Chapter 5: Simulation and experimental results**

Simulation and experimental results are given to show the effectiveness and applicability of the proposed algorithm. Several results in simulations and experiments are presented using stationary obstacle and moving obstacles.

## **Chapter 6: Conclusion**

Conclusions for this thesis and some ideas for future work are presented.



## Chapter 2: System Description

This chapter describes the prototype of the experimental differential drive automatic guided vehicle (AGV) system. This AGV prototype design consists of mechanical design, electrical design and software development. The electrical design consists of sensors, controller, actuator and power supply.

### 2.1. Mechanical Design

The AGV system used in this thesis is shown in Fig. 2.1 and the mechanical configuration is shown in Fig. 2.2.

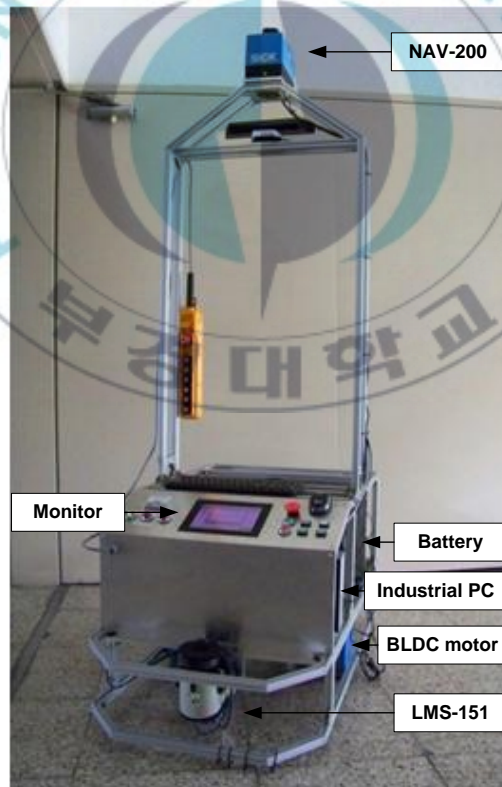


Fig. 2.1 AGV system used for the thesis.

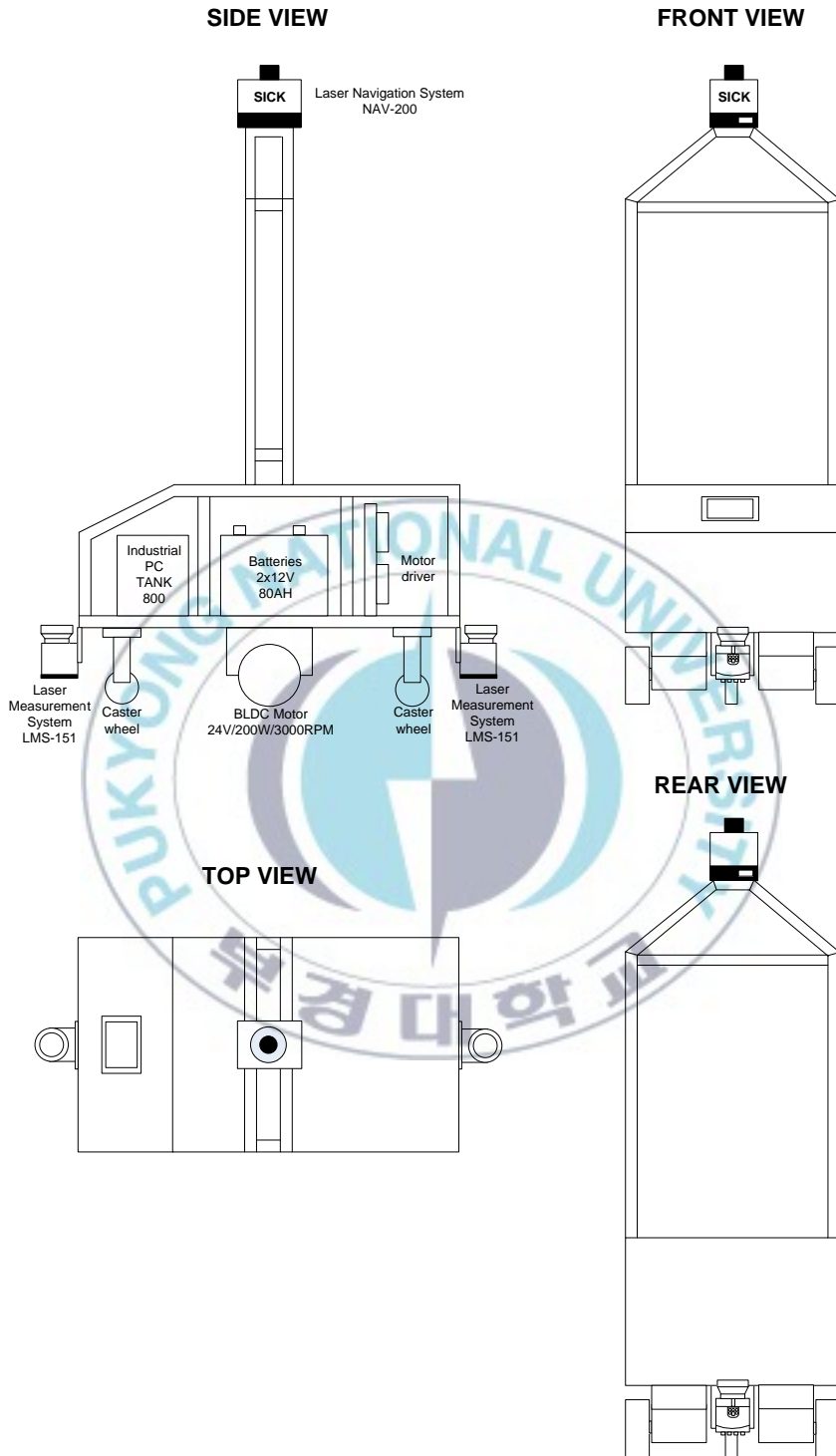


Fig. 2.2 System configuration

This AGV has dimension 60 cm x 100 cm x 190 cm. This system uses differential drive system. This system consist of two driving wheels are mounted on the left and right sides of AGV, and are driven by two BLDC motors. Two passive castor wheels are installed in front and back sides of AGV to support the AGV. The laser navigation system NAV-200 is mounted on the top of AGV. The laser measurement system LMS-151 is mounted in front and back sides of AGV. Industrial PC is placed inside the AGV platform and touch screen monitor is placed on back side of AGV. The batteries are placed on the middle of AGV. The configuration of the differential drive system is shown in Fig. 2.2.

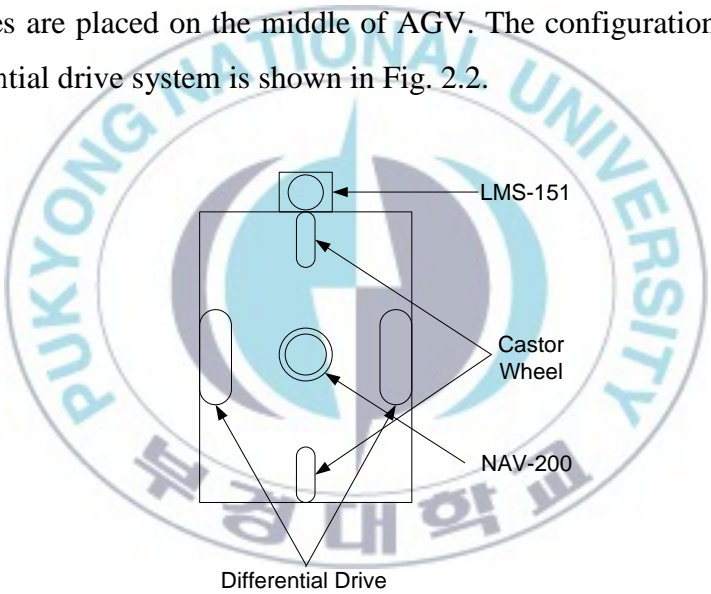


Fig. 2.3 Configuration of differential drive AGV system

## 2.2. Electrical Design

Electrical configuration of the proposed control system used for this thesis is shown in Fig. 2.4.

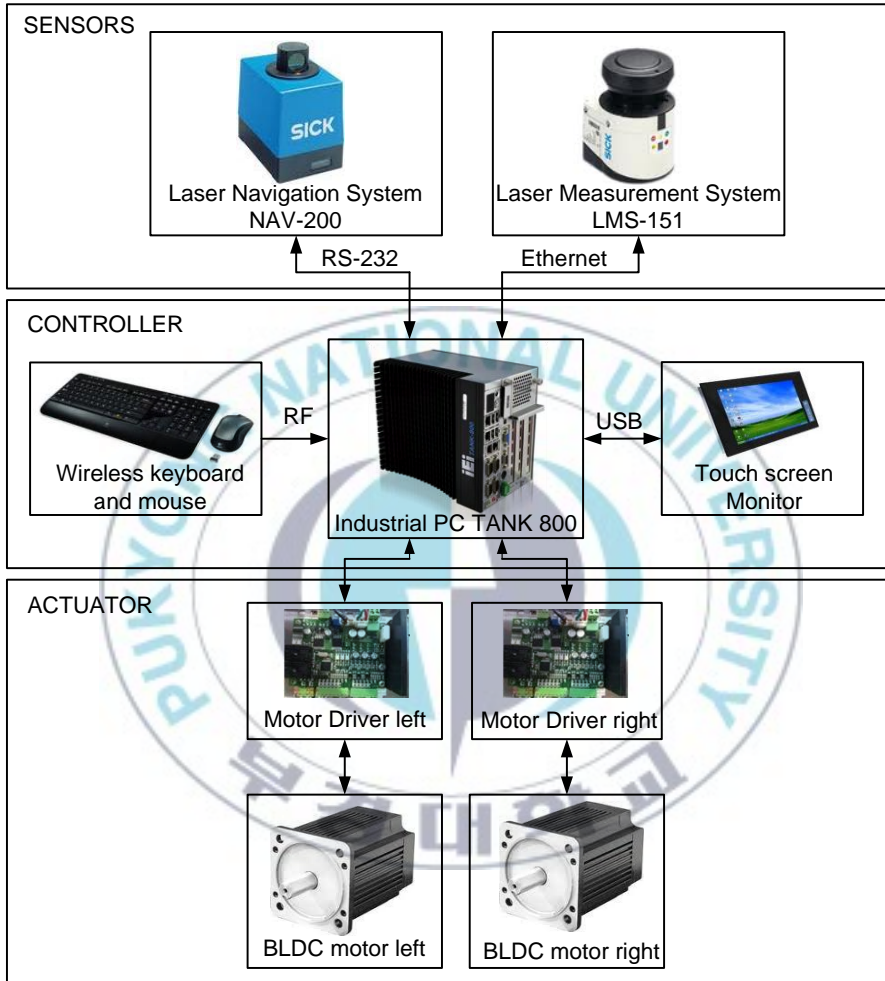


Fig. 2.4 Hardware configuration of AGV

Fig. 2.4 shows the electrical configuration of the AGV. This configuration consists of sensor part, controller part, and actuator part. The sensors part consists of laser navigation system NAV-200 and laser measurement system LMS-151. Laser navigation system NAV-

200 is connected with industrial PC via RS-232 serial data communication connections. The transmission rate is 19200 Hz. Laser measurement systems LMS-151 is connected with industrial PC via TCP/IP interface. This Ethernet interface has a transmission rate 100 Mbit. The controller part consists of industrial PC Tank 800 that is used as main controller and the wireless keyboard and mouse that are used as the input. To show the calculation and monitoring process, the touch screen monitor is used as display. The industrial PC sends analog signal and logic signals to actuator. The actuator part consists of motor driver and BLDC motor. The motor driver receives reference analog signal from controller and then it controls the speed of BLDC motor based on reference value.

### **2.2.1. Sensors**

There are two kinds of sensors that are applied in the proposed AGV system, Laser measurement system LMS-151 and laser navigation system NAV-200.

The basic principle of laser measurement system LMS-151 is shown in Fig. 2.5. The LMS transmits pulsed laser beams using a laser diode. If such a laser pulse is hit at an obstacle, it is reflected at its surface. The reflection is detected by the laser measurement system's receiver using a photodiode. The distance to the object is calculated from the propagation time ( $dt$ ) between send pulse and receive pulse that the light requires from emission to reception of the sensor.

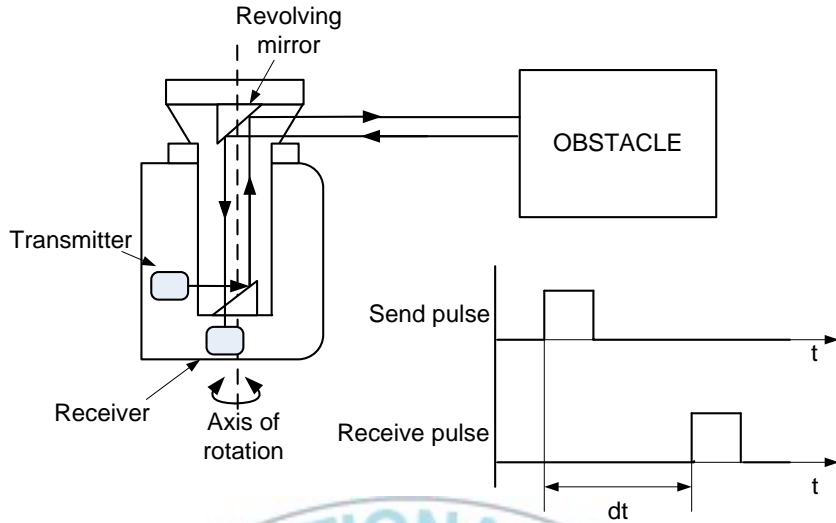


Fig. 2.5 Laser measurement system basic principle

The transmitted laser beam is deflected using a revolving mirror driven by servo motor at scanning frequency of 25 Hz and scans the surroundings in a circular manner as shown in Fig. 2.6. The scanning area defined as  $W (R_{\max}, \theta_{start}, \theta_{end})$  is given by maximum scanning distance  $R_{\max} = 50$  m, start scanning angle  $\theta_{start} = -45^\circ$  and end scanning angle  $\theta_{end} = 225^\circ$ . The measurements are triggered at regular angular steps using an angular encoder. The LMS scans with angular step ( $\Delta\theta$ ) of  $0.5^\circ$ . The DSP based scanner controller manipulates the operation of device and monitors the status of the scanner. Furthermore, the DSP sends the measurement result using ethernet protocol when the main controller of AGV requests the measurement result from LMS.

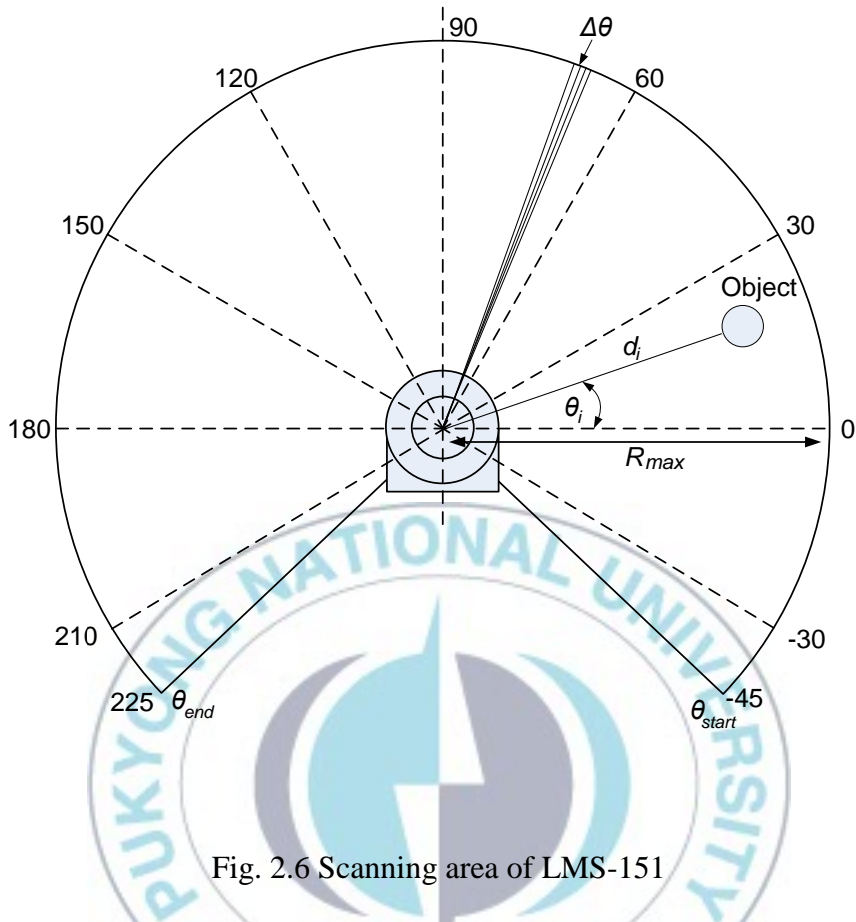


Fig. 2.6 Scanning area of LMS-151

When a single laser beam is reflected by an object as shown in Fig. 2.6, it senses the measurement distance  $d_i$  and scanning angle  $\theta_i$ . The scanning results are expressed in polar coordinate and consist of scanning angle and measurement distance as  $(d_i, \theta_i)$ . The LMS scans the environment with angular step ( $\Delta\theta$ ) of  $0.5^\circ$  and scanning area  $270^\circ$ . Therefore, in single cycle scan, it gets 540 data.

The structure of LMS-151 is shown in Fig. 2.7 and the specification of LMS-151 is shown in Table 2.1.



Fig. 2.7 Laser Measurement System LMS-151

Table 2.1 Specification of laser measurement system LMS-151

No	Parameter	Value
1	Light source	Infrared (905 nm)
2	Laser class	1 (IEC 60825-1 (2007-3))
3	Field of view	270 °
4	Scanning frequency	25 Hz / 50 Hz
5	Angular resolution	0.25°/0.5°
6	Operating range	0.5 m - 50 m
7	Data communication	Ethernet
8	Data transmission rate	100 MBit
9	Operating voltage:	10.8 V DC - 30 V DC (24 V)
10	Power consumption:	60 W
11	Weight	1.1 kg
12	Dimensions	105 mm x 102 mm x 162 mm

The second sensor used in this thesis is laser navigation system NAV-200. The basic principle of NAV-200 is shown in Fig. 2.8. Basically, the NAV-200 measures the distance in similar way with LMS-151. The NAV200 calculates its own position and orientation based on the fixed reflectors positioned (R1, R2, R3,..., Rn) in the environment, and its coordinates are detected two-dimensionally in a 360° scanning angle using a laser beam invisible to the human eye.  $n$  is the number of detected reflectors. One revolution of the scanner head here is equivalent to a scan and each revolution generates one reading per detected reflector. The measurement result are distance between sensor and reflector ( $d_1, d_2, d_3, \dots, d_n$ ) and measurement angle ( $\theta_1, \theta_2, \theta_3, \dots, \theta_n$ ).

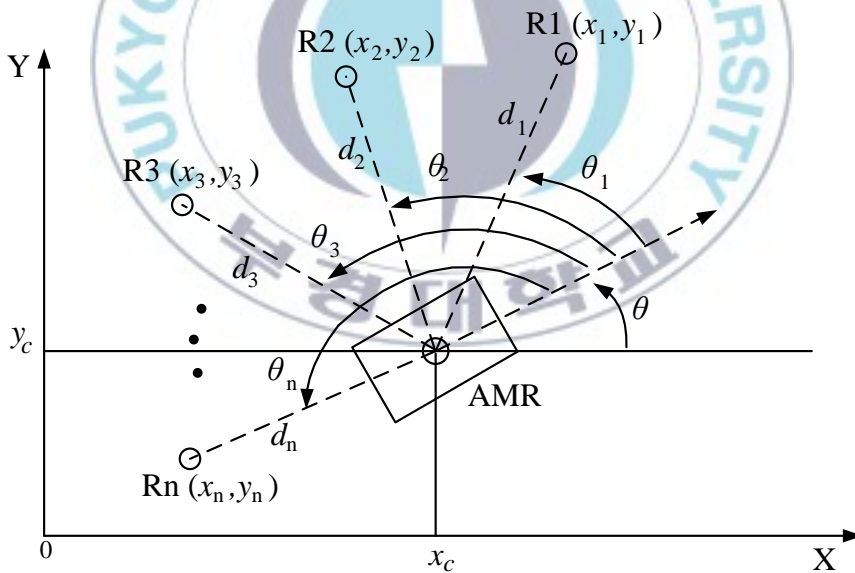


Fig. 2.8 Position measurement of the NAV-200

The coordinates of the reflectors used are stored in the nonvolatile reflector memory of the NAV200 as a reference. Three detected reflectors in a layer are sufficient for position measurement. For position measurement, the NAV200 measures the distances and angles of the reflectors and works out its own position from this data. By comparing the reflector data in the NAV memory and the measurement result, the position and orientation of AGV can be determined.

The coordinate of the AGV  $(x_c, y_c)$  and its orientation  $\theta$  can be obtained from [40] as follows:

$$x_c = \left[ \frac{1}{(m_2 - m_1)(1 + m^2)} \right] \left\{ (m_2 m - 1) \times [(m_1 + m)x_1 + (m_1 m - 1)y_1] - (m_1 m - 1) \times [(m_2 + m)x_2 + (m_2 m - 1)y_2] \right\} \quad (2.1)$$

$$y_c = \left[ \frac{1}{(m_2 - m_1)(1 + m^2)} \right] \left\{ (m_1 + m) \times [(m_2 + m)x_2 + (m_2 m - 1)y_2] - (m_2 + m) \times [(m_1 + m)x_1 + (m_1 m - 1)y_1] \right\} \quad (2.2)$$

$$\theta = \text{Atan}2(y_1 - y_c, x_1 - x_c) - \theta_1 \quad (2.3)$$

where  $m_1 = \tan \theta_1$ ,  $m_2 = \tan \theta_2$ ,  $m_3 = \tan \theta_3$  and  $m = \tan \theta$ .

From Eqs. (2.1) ~ (2.3),  $m$  is given by:

$$m = \frac{(m_3 - m_1)(y_1 - y_2 - m_1 x_1 + m_2 x_2) - (m_2 - m_1)(y_1 - y_3 - m_1 x_1 + m_3 x_3)}{(m_3 - m_1)(m_1 y_1 + x_1 - m_2 y_2 - x_2) - (m_2 - m_1)(m_1 y_1 + x_1 - m_3 y_3 - x_3)} \quad (2.4)$$

The structure of laser navigation system NAV-200 is shown in Fig. 2.9.



**Legend:**

- |   |  |
|---|--|
| ① Scanner head, rotating                      | ⑦ "RS 232 data interface" connection (14-pin chassis-mount plug) |
| ② Light outlet/inlet aperture                 | ⑧ "Power Supply 24 V DC" connection (8-pin chassis-mount plug)   |
| ③ Status indicator (LEDs 4 x)                 | ⑨ Fuse (3.15 A slow-blow)  |
| ④ RS 232 data cable (see Table 10-3, Page 80) | ⑩ Functional earth terminal                                      |
| ⑤ 9-pin D-Sub socket for Host/PC connection   | ⑪ Tapped holes in baseplate (4 x) (not visible here)             |
| ⑥ 14-pin cable socket for                     | ⑫ Laser warning label  |
|   | ⑬ 8-pin cable socket   |

Fig. 2.9 Laser navigation system NAV-200

The specification of laser navigation system NAV-200 is shown in Table 2.2.

Table 2.2 Specification of Laser navigation system NAV-200

No	Parameter	Value
1	Light source	Infrared (855 nm)
2	Laser class	1
3	Field of view	360 °
4	Scanning frequency	8 Hz
5	Angular resolution	0.1°
6	Operating range	1.2 m – 28.5 m
7	Max. range 10 % reflectivity	28.5 m
8	Data communication	Serial (RS-232)
9	Data transmission rate	19200 Hz
10	Operating voltage:	$\geq 24 \text{ V DC} \pm 25\%$
11	Power consumption:	24 W
12	Weight	3.3 kg
13	Dimensions	176 mm x 178 mm x 115 mm

### 2.2.2. Controller

In this thesis, industrial PC TANK-800 of the controller part is used as main controller. The structure of industrial PC used as a controller for this thesis is shown in Fig. 2.10.

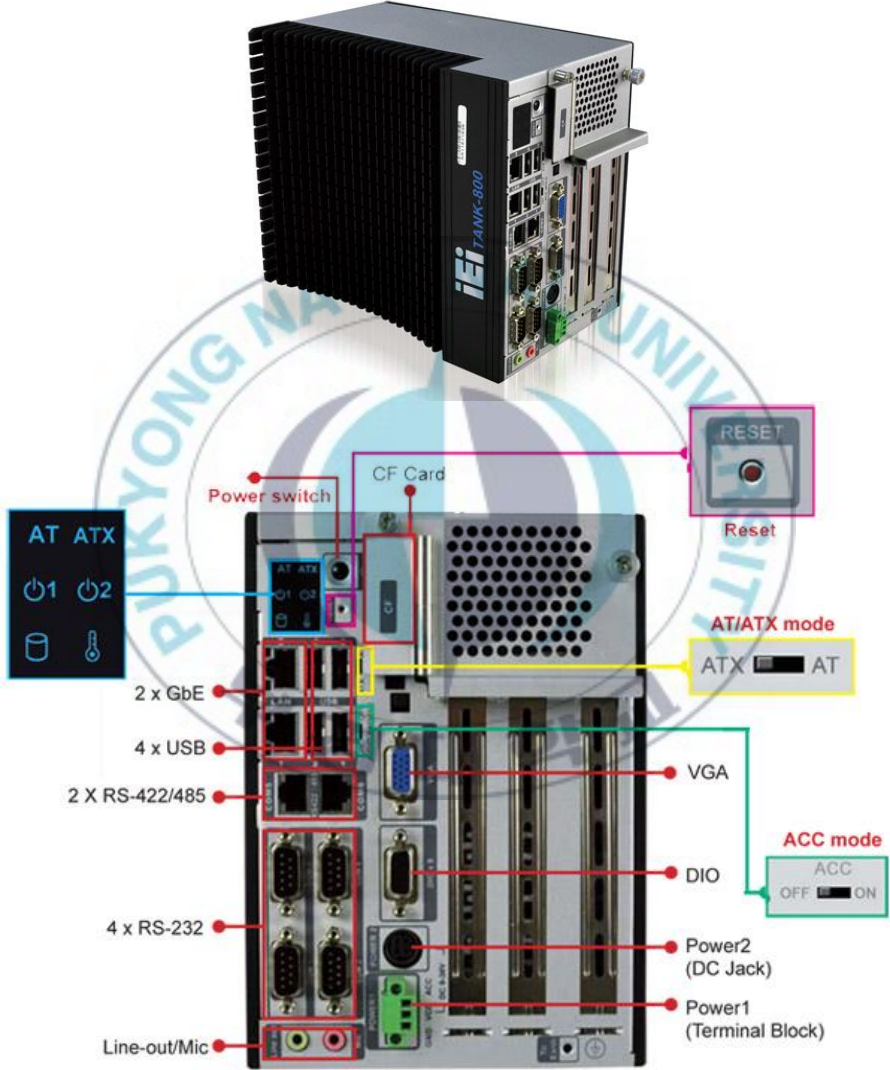


Fig. 2.10 Industrial PC TANK-800

The specification of Industrial PC TANK-800 is shown in Table 2.3.

Table 2.3 Specification of PC TANK-800

No	Parameter		Value
1	Chassis	Dimensions	136 mm x 219 mm x 188 mm
2	Motherboard	CPU	Intel® Atom™ D525 1.8GHz dual-core processor
		Chipset	Intel® ICH8M
		Ethernet	Dual Realtek RTL8111E PCIe GbE controllers support ASF 2.0
3	Storage	SATA	2.5" SATA HDD bay
4	System Function	USB	4 x USB 2.0
		Ethernet	2 x RJ-45
		RS-232	4 x DB-9
		RS-422/485	2 x RJ-45
		Display	1 x VGA
		Resolution	Up to 2048x1536
		Audio	1 x Mic-in, 1 x Line-out
		DIO	1 x DB-9
		Interior Expansions	One PCIe x4 (physical one PCIe x16 slot) and two PCI slots
5	Power	Power Supply	10.5V (+/-0.3V) ~ 36V
		Power Consumption	33W (without add-on card)
6	Reliability	Operating Temperature	-20°C ~ 70°C
		Weight	3.0Kg

### 2.2.3. Actuator

The actuator consists of motor driver and BLDC motor. Each motor uses 24VDC power supply. The maximum current allowed by motor driver is 20A. The motor driver used for this thesis shown in Fig. 2.11.

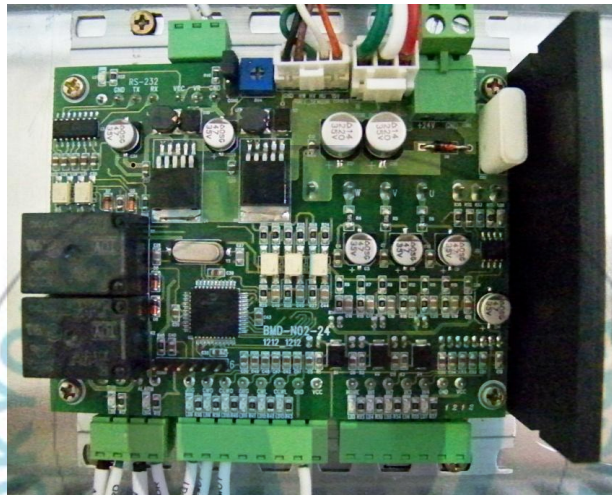


Fig. 2.11 Motor driver

The structure of BLDC motor used for this thesis is shown in Fig. 2.12.



Fig. 2.12 BLDC motor

The specification of BLDC motor SWIS BG90-S024 is shown in Table 2.4.

Table 2.4 Specification of BLDC motor SWIS BG90-S024

No	Parameter	Rating
1	Rated Voltage	24 V
2	Rated Output	200 W
3	Rated Current	11.9 A
4	Rated Speed	3000 RPM
5	Rated Torque	6.3 Kgf-cm
6	Weight	2.7 Kg
7	Voltage constant	14.8 v/Krpm
8	Torque Constant	1.4 kgf.cm
9	Rotor inertia	$0.24 \times 10^{-3} \text{ kg.m}^2$
9	Armature resistance	0.9 ohm
10	Armature inductance	0.9 mH
11	Mechanical time constant	10 ms
12	Electrical time constant	1.1ms

#### 2.2.4. Power supply

In AGV system, all devices need 24V power supply. The battery structure is shown in Fig. 2.13. The specification of battery Rocket AGM 80-12 is shown in Table 2.5.



Fig. 2.13 Structure of Battery

Table 2.5 Battery Rocket AGM 80-12 parameters

No	Parameter	Value	
1	Nominal Voltage (V)	12 V	
2	Capacity (AH)	10HR 1.80(V/Cell)	80.0 AH
		5 HR 1.70 (V/Cell)	68.0 AH
		3 HR 1.67 (V/Cell)	61.5 AH
		1 HR 1.60 (V/Cell)	48.0 AH
		0.5 HR 1.60 (V/Cell)	37.5 AH
3	Dimension (mm)	Length	332 mm
		Width	174 mm
		Height	229 mm
		Total Height	229 mm
4	Weight	24.7 Kg	
5	Terminal type	Bolt terminal	

### 2.3. Software development

In this thesis, a program to control entire AGV system is developed using C# programming language of Visual Studio 2008. This program requests the position data from NAV-200 and obstacle scanning data from LMS-151. Based on the information data from the sensors, the navigation algorithm using tangent bug gives the direction of AGV movement. If the obstacles are detected, the program calculates the avoidance path by the proposed obstacle avoidance algorithm. This program also controls the velocity of the actuators by sending the analog reference value for motor driver.

The flowchart of the program is shown in Fig. 2.14 and the flowchart for obstacle avoidance algorithm is shown in Fig. 2.15.

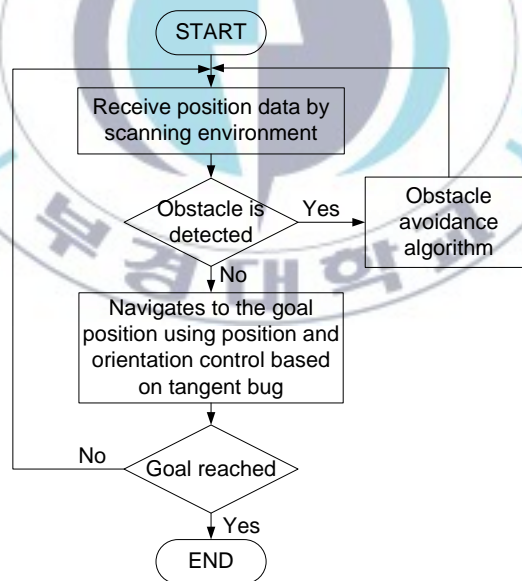


Fig. 2.14 Flowchart program of the AGV

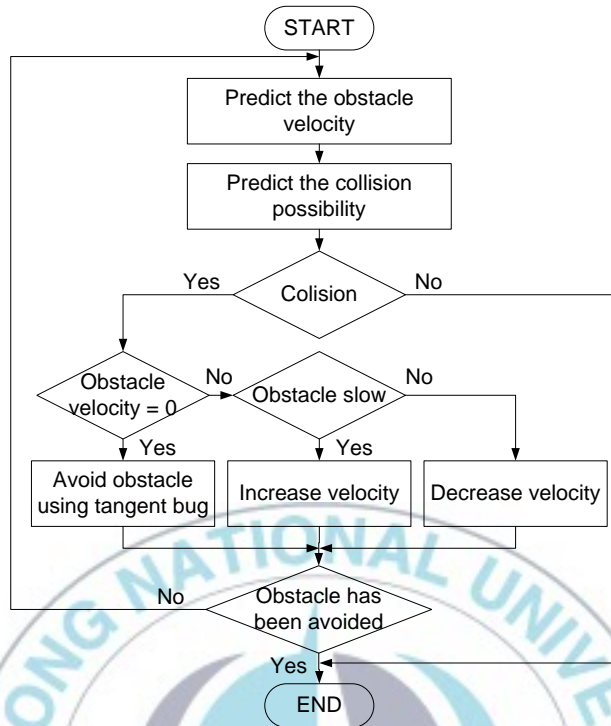


Fig. 2.15 Flowchart of obstacle avoidance algorithm

Fig. 2.16 shows the interface of the program on the industrial PC.

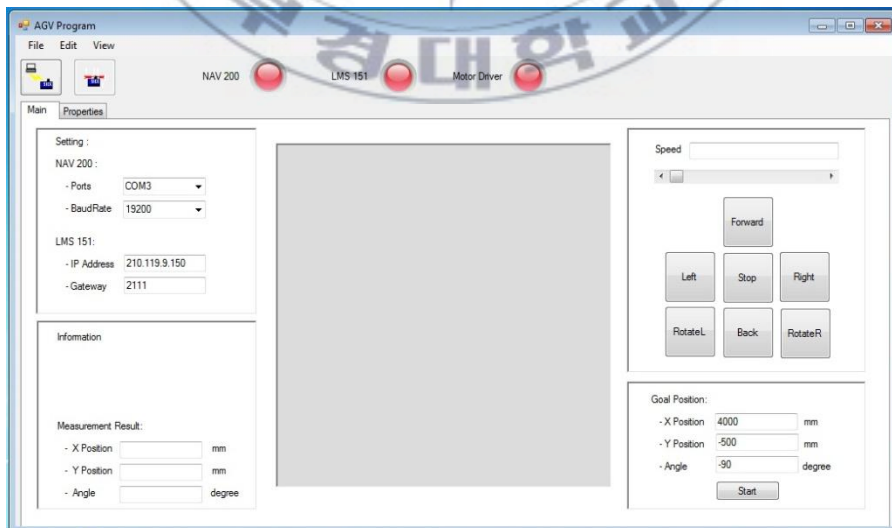
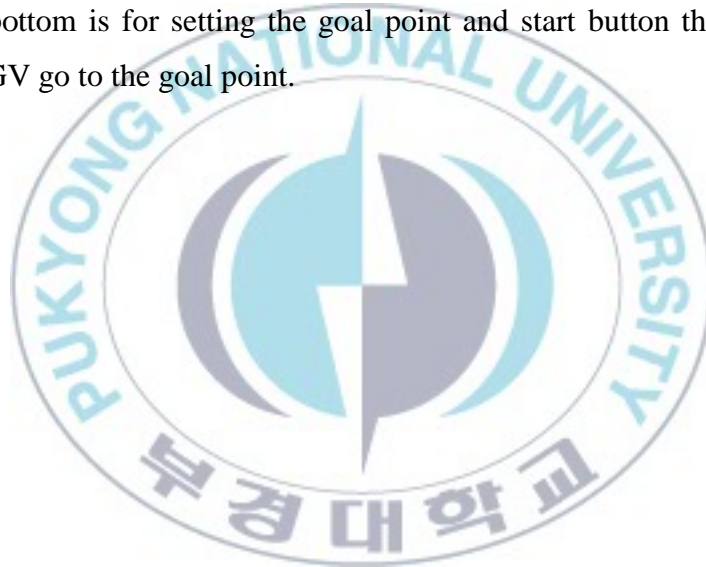


Fig. 2.16 Interface of AGV program

On the Interface at Fig. 2.16, there are 5 partitions. On the top, there are connection buttons to connect the computer to the sensors and LED as connection indicator with the sensors and actuator. The first partition on the top left is for setting the connection with the sensors. The second partition on the bottom left is for displaying position measurement result from NAV-200. The third partition on the middle shows the scanned environment using the measurement result of LMS-151. The fourth partition on the top right is for controlling the movement of AGV manually. The last partition on the right bottom is for setting the goal point and start button that make the AGV go to the goal point.



## Chapter 3: System Modeling

This chapter presents the mathematical modeling of the proposed AGV system. The mathematic modeling consists of kinematic modeling and dynamic modeling. The AGV used in this thesis has two driving wheels on the left and right sides of AGV are driven by BLDC motor. Two passive castor wheels are installed on the front and back sides of AGV to balance the AGV.

Fig. 3.1 show the coordinate for AGV's modeling where  $XOY$  is the global coordinate and  $xCy$  is moving coordinate of AGV.

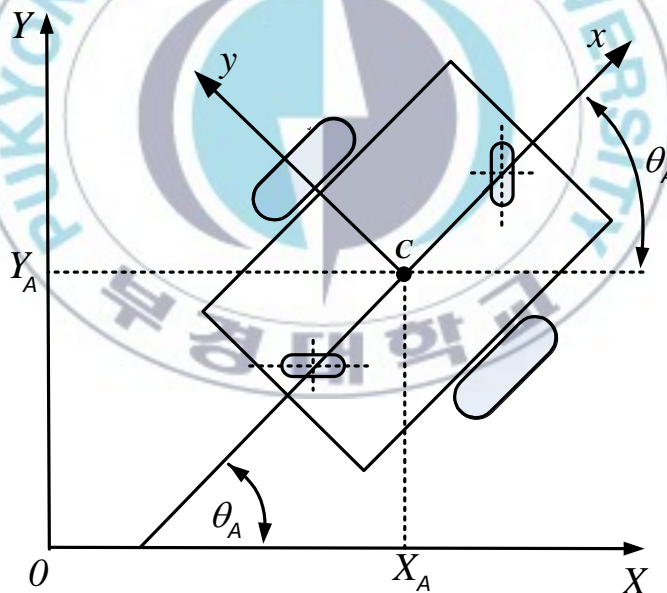


Fig. 3.1 Coordinate of AGV's modeling

To specify the position of the AGV, a point C on the AGV's chassis is chosen as its position reference point. The position of C in the global reference frame is specified by coordinates  $X_A$  and  $Y_A$ , and the angular difference between the global and local reference frames is given by  $\theta_A$ .

$\xi_1$  is described as a position vector with position and orientation of the AGV in global coordinate:

$$\xi_1 = \begin{bmatrix} X_A \\ Y_A \\ \theta_A \end{bmatrix} \quad (3.1)$$

Relation of AGV's position vector  $\xi_1$  in global coordinate  $XOY$  and its position vector  $\xi_A$  in local coordinate  $xCy$  is described by:

$$\xi_A = R(\theta_A)\xi_1 \quad (3.2)$$

where  $R(\theta_A)$  is the orthogonal rotational matrix (3x3)

$$R(\theta_A) = \begin{bmatrix} \cos \theta_A & \sin \theta_A & 0 \\ -\sin \theta_A & \cos \theta_A & 0 \\ 0 & 0 & 1 \end{bmatrix} \quad (3.3)$$

### 3.1. Characterization of wheels

#### 3.1.1. Fixed standard wheel for driving wheel

The fixed standard wheel has no vertical axis of rotation for steering. Its angle to the chassis is fixed, and it is limited to motion back and forth along the wheel plane and rotation around its contact point with the ground plane. Fig. 3.2 depicts a fixed standard wheel and indicates its position relative to the AGV's local coordinate frame  $xCy$ . The position of the wheel is expressed in polar coordinates by distance ( $l$ ) and angle ( $\alpha$ ). The angle of the wheel plane relative to the chassis is denoted by  $\beta$ , which is fixed since the fixed standard wheel is not steerable. The wheel with radius  $r$  can spin over time, and so its rotational angle around its horizontal axle is a function of time  $t$ :  $\varphi(t)$ .

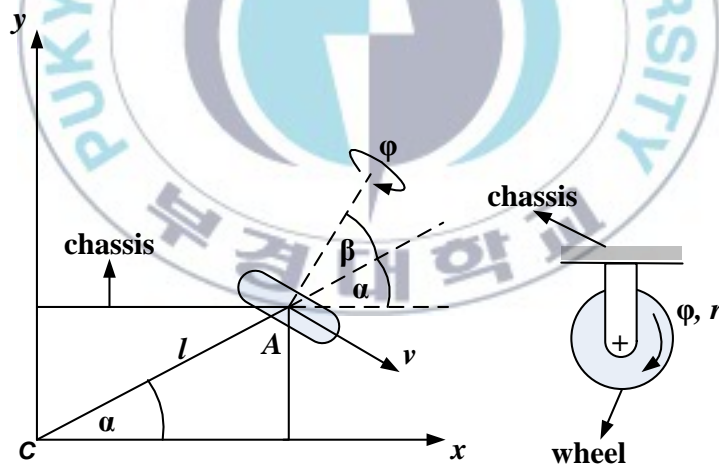


Fig. 3.2 A fixed standard wheel and its parameters

The rolling constraint for this wheel enforces that all motion along the direction of the wheel plane must be accompanied by the appropriate amount of wheel spin so that there is pure rolling at the contact point:

$$[\sin(\alpha + \beta) \quad \{-\cos(\alpha + \beta)\} \quad (-l)\cos\beta] R(\theta_A) \dot{\xi}_1 - r\dot{\phi} = 0 \quad (3.4)$$

The sliding constraint for this wheel enforces that the component of the wheel's motion orthogonal to the wheel plane must be zero.

$$[\cos(\alpha + \beta) \quad \sin(\alpha + \beta) \quad l\sin\beta] R(\theta_A) \dot{\xi}_1 = 0 \quad (3.5)$$

### 3.1.2. Castor wheel

Castor wheels are able to steer around a vertical axis. However, unlike the standard wheel, the vertical axis of rotation in a castor wheel does not pass through the ground contact point. Fig. 3.3 depicts a castor wheel, demonstrating that formal specification of the castor wheel's position requires an additional parameter. The wheel contact point is now at position  $B$ , which is connected by a fixed length rigid rod  $AB$  to the vertical axis point  $A$  fixed on the chassis. Point  $A$  has a position specified in the robot's reference frame as in Fig. 3.3. It is assumed that the plane of the wheel is aligned with  $AB$  at all times. Similarly to the steered standard wheel, the castor wheel has two parameters that vary as a function of time.  $\phi(t)$  represents the wheel rotation angle over time.  $\beta(t)$  denotes the steering angle and orientation of  $AB$  over time.

Because the offset axis plays no role during motion that is aligned with the wheel plane for the castor wheel, the rolling constraint is:

$$[\sin(\alpha + \beta) \quad \{-\cos(\alpha + \beta)\} \quad (-l)\cos\beta] R(\theta_A) \dot{\xi}_1 - r\dot{\phi} = 0 \quad (3.6)$$

The sliding constraint of castor wheel is:

$$[\cos(\alpha + \beta) \quad \sin(\alpha + \beta) \quad l \sin \beta] R(\theta_A) \dot{\xi}_1 = 0 \quad (3.7)$$

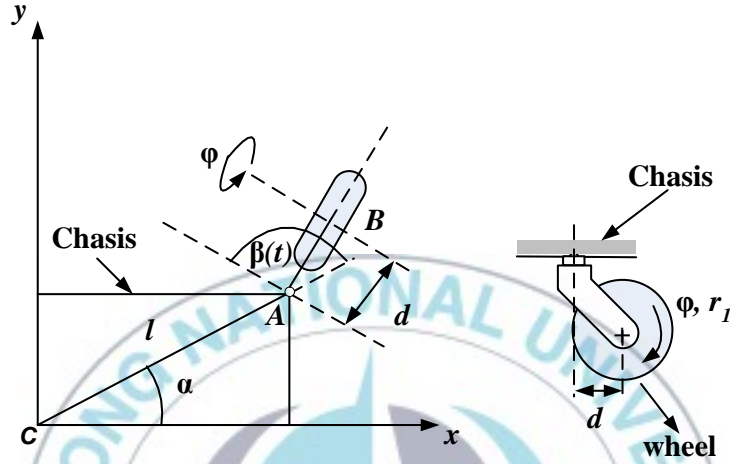


Fig. 3.3 A castor wheel and its parameters

### 3.2. Kinematic modeling of differential drive AGV system

The schematic modeling of differential drive AGV system is shown in Fig. 3.4. As shown in Fig. 3.4, the AGV position in global coordinate XOY is  $(X_A, Y_A)$  with orientation angle  $\theta_A$  measured from X axis of global coordinate. The AGV moves with linear velocity  $V_A$  and angular velocity  $\omega_A$ . This differential drive AGV has two driving standard wheels  $W1$  and  $W2$  with radius  $r$ , located in y axis of local coordinate AGV. Linear velocities of the left wheel and the right wheel are denoted by  $v_L$  and  $v_R$ , respectively. Given a point C centered between the two drive wheels, each wheel is a distance  $l$  from C. The castor wheels  $W3$  and  $W4$  are located in x axis of local

coordinate AGV. The castor wheels impose no kinematic constraints on the robot chassis, since it unpowered and can move freely in all direction. Therefore, only two driving standard wheels  $W1$  and  $W2$  have impact on AGV kinematics and are considered in computing the AGV's kinematic constraints.

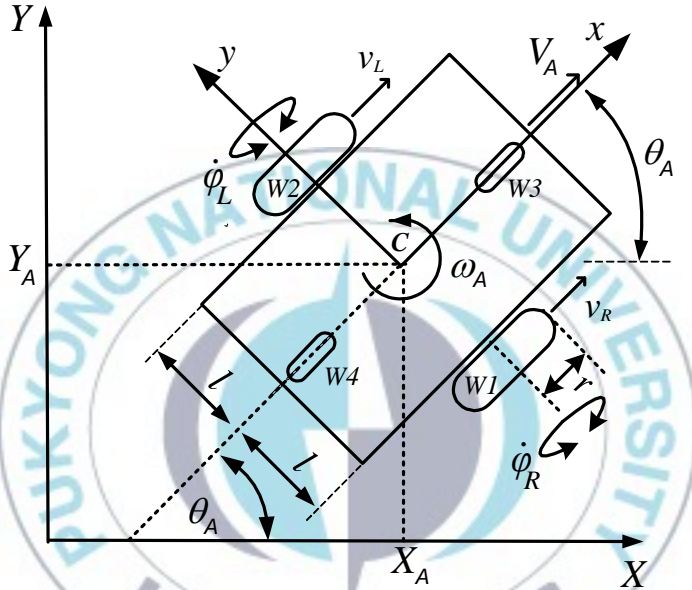


Fig. 3.4 Coordinate of differential drive AGV system

From Fig. 3.4, parameters of the right wheel  $W1$  are  $\alpha = -\pi/2$ ,  $\beta = \pi$  and parameters of left wheel  $W2$  are  $\alpha = \pi/2$ ,  $\beta = 0$ . Eq. (3.4) of the rolling constraints with respect to the left and right wheels can be calculated as:

$$\begin{bmatrix} \sin(-\pi/2 + \pi) & \{-\cos(-\pi/2 + \pi)\} & (-l) \cos \pi \\ \sin(\pi/2 + 0) & \{-\cos(\pi/2 + 0)\} & (-l) \cos 0 \end{bmatrix} R(\theta_A) \dot{\xi}_1 - \begin{bmatrix} r & 0 \\ 0 & r \end{bmatrix} \dot{\phi} = 0 \quad (3.8)$$

where  $\dot{\phi} = [\dot{\phi}_R \quad \dot{\phi}_L]^T$ , and  $r$  is radius of driving wheels.

Eq. (3.8) can be written as:

$$\begin{bmatrix} 1 & 0 & l \\ 1 & 0 & -l \end{bmatrix} R(\theta_A) \dot{\xi}_1 = \begin{bmatrix} r & 0 \\ 0 & r \end{bmatrix} \dot{\phi} \quad (3.9)$$

For the sliding constraint, because the two driving wheels are parallel, Eq. (3.5) results in only one independent equation. Using parameters of the right wheel W1,  $\alpha = -\pi/2$ , and  $\beta = \pi$ , the sliding constraints can be calculated as:

$$\begin{bmatrix} \cos(-\pi/2 + \pi) & \sin(-\pi/2 + \pi) & l \sin \pi \end{bmatrix} R(\theta_A) \dot{\xi}_1 = 0 \quad (3.10)$$

Eq. (3.10) can be written as:

$$\begin{bmatrix} 0 & 1 & 0 \end{bmatrix} R(\theta_A) \dot{\xi}_1 = 0 \quad (3.11)$$

The AGV's equation related to the rolling and sliding constraints and the wheel angular velocity vector of the AGV's wheels  $\dot{\phi}$  is expressed by:

$$\begin{bmatrix} J_1(\beta) \\ C_1(\beta) \end{bmatrix} R(\theta_A) \dot{\xi}_1 = \begin{bmatrix} J_2 \dot{\phi} \\ 0 \end{bmatrix} \quad (3.12)$$

$$\text{where } J_1(\beta) = \begin{bmatrix} 1 & 0 & l \\ 1 & 0 & -l \end{bmatrix}, \quad C_1(\beta) = \begin{bmatrix} 0 & 1 & 0 \end{bmatrix} \text{ and } J_2 = \begin{bmatrix} r & 0 \\ 0 & r \end{bmatrix}$$

By combining Eqs. (3.9) and (3.11), the rolling constraints of all wheels can now be collected in a single expression:

$$\begin{bmatrix} 1 & 0 & l \\ 1 & 0 & -l \\ 0 & 1 & 0 \end{bmatrix} R(\theta_A) \dot{\xi}_I = \begin{bmatrix} J_2 \dot{\phi} \\ 0 \end{bmatrix} \quad (3.13)$$

From Eq. (3.13), the kinematic equation of differential drive AGV can be obtained as:

$$\dot{\xi}_I = R(\theta_A)^{-1} \begin{bmatrix} 1 & 0 & l \\ 1 & 0 & -l \\ 0 & 1 & 0 \end{bmatrix}^{-1} \begin{bmatrix} J_2 \dot{\phi} \\ 0 \end{bmatrix} = R(\theta_A)^{-1} \begin{bmatrix} \frac{1}{2} & \frac{1}{2} & 0 \\ 0 & 0 & 1 \\ \frac{1}{2l} & -\frac{1}{2l} & 0 \end{bmatrix} \begin{bmatrix} J_2 \dot{\phi} \\ 0 \end{bmatrix} \quad (3.14)$$

$$\dot{\xi}_I = \begin{bmatrix} \dot{X}_A \\ \dot{Y}_A \\ \dot{\theta}_A \end{bmatrix} = R(\theta_A)^{-1} \begin{bmatrix} \frac{r\dot{\phi}_R + r\dot{\phi}_L}{2} \\ 0 \\ \frac{r\dot{\phi}_R - r\dot{\phi}_L}{2l} \end{bmatrix} \quad (3.15)$$

$$\text{where } R(\theta_A)^{-1} = \begin{bmatrix} \cos \theta_A & -\sin \theta_A & 0 \\ \sin \theta_A & \cos \theta_A & 0 \\ 0 & 0 & 1 \end{bmatrix}$$

As shown in Eq. (3.15), velocity of the AGV in Y axis direction is always 0. Therefore, Eq. (3.15) can be expressed into

$$\dot{\xi}_I = \begin{bmatrix} \dot{X}_A \\ \dot{Y}_A \\ \dot{\theta}_A \end{bmatrix} = \begin{bmatrix} \cos \theta_A & 0 \\ \sin \theta_A & 0 \\ 0 & 1 \end{bmatrix} \begin{bmatrix} \frac{r\dot{\phi}_R + r\dot{\phi}_L}{2} \\ \frac{r\dot{\phi}_R - r\dot{\phi}_L}{2l} \end{bmatrix} \quad (3.16)$$

Therefore, kinematic equation Eq. (3.16), of the AGV also can be expressed in term of its linear velocity ( $V_A$ ) and angular velocity ( $\omega_A$ ) are shown as follows:

$$\dot{\xi}_I = \begin{bmatrix} \dot{X}_A \\ \dot{Y}_A \\ \dot{\theta}_A \end{bmatrix} = \begin{bmatrix} \cos \theta_A & 0 \\ \sin \theta_A & 0 \\ 0 & 1 \end{bmatrix} \begin{bmatrix} V_A \\ \omega_A \end{bmatrix} \quad (3.17)$$

From Eqs. (3.16) and (3.17), the relation between AGV's velocities and left and right wheel angular velocities can be expressed as:

$$\begin{bmatrix} V_A \\ \omega_A \end{bmatrix} = \begin{bmatrix} \frac{r}{2} & \frac{r}{2} \\ \frac{r}{2l} & \frac{-r}{2l} \end{bmatrix} \begin{bmatrix} \dot{\phi}_R \\ \dot{\phi}_L \end{bmatrix} \quad (3.18)$$

or vice versa,

$$\begin{bmatrix} \dot{\phi}_R \\ \dot{\phi}_L \end{bmatrix} = \begin{bmatrix} \frac{r}{2} & \frac{r}{2} \\ \frac{r}{2l} & \frac{-r}{2l} \end{bmatrix}^{-1} \begin{bmatrix} V_A \\ \omega_A \end{bmatrix} \quad (3.19)$$

In Fig. 3.5, the error vector  $\mathbf{e}=[e_1, e_2]^T$  is defined as the difference between the current AGV velocity and orientation and the reference velocity and orientation.

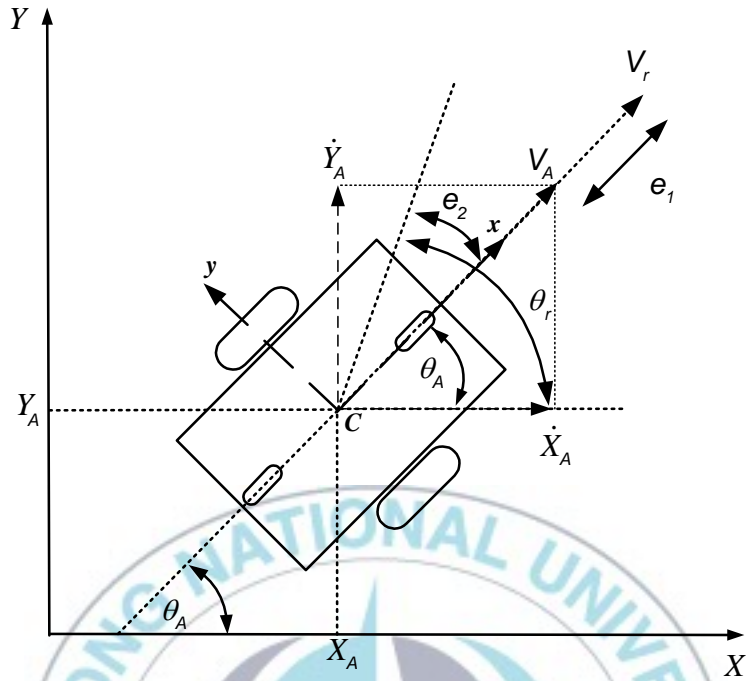


Fig. 3.5 Definition of error in proposed AGV system

The output velocities of AGV can be expressed as:

$$\begin{bmatrix} V_A \\ \omega_A \end{bmatrix} = \begin{bmatrix} \cos \theta_A & \sin \theta_A & 0 \\ 0 & 0 & 1 \end{bmatrix} \begin{bmatrix} \dot{X}_A \\ \dot{Y}_A \\ \dot{\theta}_A \end{bmatrix} \quad (3.20)$$

Velocity error vector are defined as the differences between the reference velocity and the current velocity of AGV as follows:

$$\mathbf{e} = \begin{bmatrix} e_1 \\ e_2 \end{bmatrix} = \begin{bmatrix} V_A - V_r \\ \omega_A - \omega_r \end{bmatrix} \quad (3.21)$$

where  $e_1$ ,  $e_2$  are linear velocity error and angular velocity error of AGV, respectively.

By combining Eqs. (3.19) and (3.21), the angular velocity error of each wheel can be obtained as follows:

$$\begin{bmatrix} \dot{\phi}_{eR} \\ \dot{\phi}_{eL} \end{bmatrix} = \begin{bmatrix} \frac{r}{2} & \frac{r}{2} \\ \frac{r}{2l} & \frac{r}{2l} \end{bmatrix}^{-1} \begin{bmatrix} e_1 \\ e_2 \end{bmatrix} \quad (3.22)$$

### 3.3. BLDC motor modeling

From Eq. (3.15), the position of AGV is related directly with standard driving wheel velocities  $\dot{\phi}_R$  and  $\dot{\phi}_L$ . Furthermore, the AGV linear velocity and orientation can be controlled by changing the wheel velocities. In this thesis, brushless direct current (BLDC) motors are used as actuator. Because the modelings of the BLDC motors of left and right wheels are same, the following modeling with respect to one motor is introduced.

Fig. 3.6 shows a typical BLDC motor system arrangement for each left and right wheel. The basic schematic of BLDC motor is represented by the armature resistance  $R$ , the armature inductance  $L$  and back emf  $E$ .

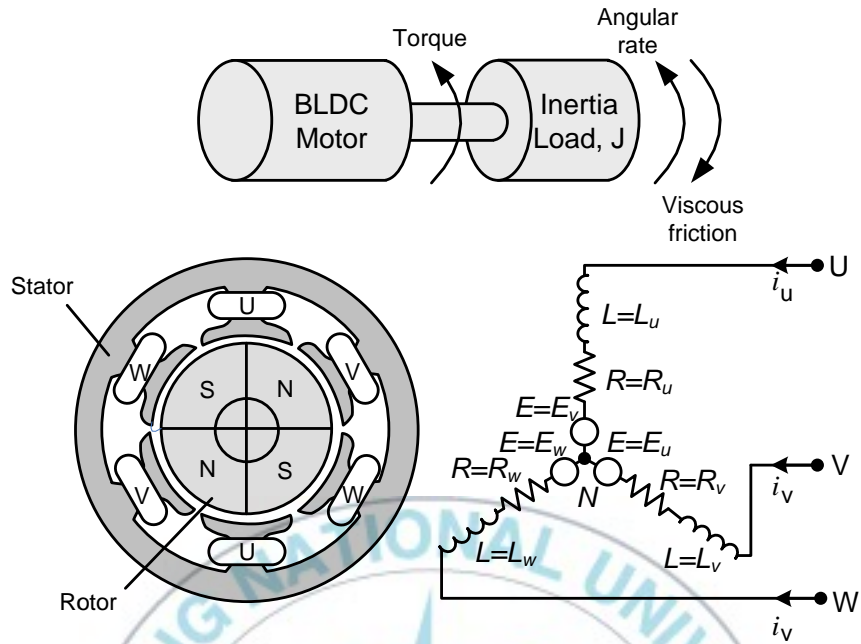


Fig. 3.6 A typical BLDC motor system arrangement

From Fig. 3.6, the following equations are used to describe the relationship of operation. For each phase, using Kirchoff's voltage law (KVL), the following equation is obtained:

$$V_s = Ri + L \frac{di}{dt} + E \quad (3.23)$$

where  $V_s = V_{UN} = V_{VN} = V_{WN}$  is the DC voltage source and  $i = i_u = i_v = i_w$  is the armature current

Eq. (3.23) is rearranged as follows:

$$\frac{di}{dt} = -i \frac{R}{L} - \frac{E}{L} + \frac{1}{L} V_s \quad (3.24)$$

From Newton's second law of motion, the following dynamic equation is obtained.

$$J \frac{d\dot{\phi}}{dt} = \sum T_i \quad (3.25)$$

$$T_e = k_f \dot{\phi} + J \frac{d\dot{\phi}}{dt} + T_L \quad (3.26)$$

where,

$T_e$  = electrical torque (N)

$k_f$  = friction constant (Nms)

$J$  = inertia moment of rotor (kg.m<sup>2</sup>)

$\dot{\phi} = \dot{\phi}_R = \dot{\phi}_L$  = angular velocity (rad)

$T_L$  = mechanical load torque (N)

where the back emf and the electrical torque can be written as:

$$E = k_e \dot{\phi} \text{ and } T_e = k_t \dot{\phi} \quad (3.27)$$

where  $k_e$  is the back emf constant and  $k_t$  is the torque constant.

From Eqs. (3.24) ~ (3.27), Eq. (3.28) and Eq. (3.29) are obtained.

$$\frac{di}{dt} = -i \frac{R}{L} - \frac{k_e}{L} \dot{\phi} + \frac{1}{L} V_s \quad (3.28)$$

$$\frac{d\dot{\phi}}{dt} = i \frac{k_t}{J} - \frac{k_f}{J} \dot{\phi} + \frac{1}{J} T_L \quad (3.29)$$

Using Laplace transform, Eqs. (3.28) ~ (3.29) are transformed as follows:

$$si = -i\frac{R}{L} - \frac{k_e}{L}\dot{\phi} + \frac{1}{L}V_s \quad (3.30)$$

$$s\dot{\phi} = i\frac{k_t}{J} - \frac{k_f}{J}\dot{\phi} + \frac{1}{J}T_L \quad (3.31)$$

At no load  $T_L = 0$ , Eq. (3.31) becomes:

$$s\dot{\phi} = i\frac{k_t}{J} - \frac{k_f}{J}\dot{\phi} \quad (3.32)$$

Substituting Eq. (3.32) into Eq. (3.30) yields:

$$\left( \frac{s\dot{\phi} + \frac{k_f}{J}\dot{\phi}}{\frac{k_t}{J}} \right) \left( s + \frac{R}{L} \right) = -\frac{k_e}{L}\dot{\phi} + \frac{1}{L}V_s \quad (3.33)$$

$$\left\{ \left( \frac{s^2J}{k_t} + \frac{sk_f}{k_t} + \frac{sRJ}{k_tL} + \frac{k_fR}{k_tL} \right) + \frac{k_e}{L} \right\} \dot{\phi} = \frac{1}{L}V_s \quad (3.34)$$

$$V_s = \left\{ \frac{s^2JL + sk_fL + sRJ + k_fR + k_ek_t}{k_t} \right\} \dot{\phi} \quad (3.35)$$

The transfer function represented as the ratio of the angular velocity  $\dot{\phi}$  as output to source voltage  $V_s$  as input is obtained as follows:

$$G(s) = \frac{\dot{\phi}}{V_s} = \frac{k_t}{s^2 JL + (RJ + k_f L)s + k_f R + k_e k_t} \quad (3.36)$$

The following assumptions are given:

1. The friction constant is small. That is,  $k_f$  tends to 0.
2.  $RJ \gg k_f L$
3.  $k_e k_t \gg k_f R$

The transfer function is finally written as:

$$G(s) = \frac{\dot{\phi}}{V_s} = \frac{k_t}{s^2 JL + RJ s + k_e k_t} \quad (3.37)$$

Eq. (3.37) is rewritten as:

$$G(s) = \frac{\dot{\phi}}{V_s} = \frac{\frac{1}{k_e}}{\frac{RJ}{k_e k_t} \cdot \frac{L}{R} \cdot s^2 + \frac{RJ}{k_e k_t} \cdot s + 1} \quad (3.38)$$

Since the BLDC consists of three phases, the mechanical and electrical constants become:

Mechanical constant:

$$\tau_m = \frac{R_t J}{k_e k_t} = \frac{J \cdot (R_u + R_v + R_w)}{k_e k_t} = \frac{J \cdot 3R}{k_e k_t} \quad (3.39)$$

Electrical constant:

$$\tau_e = \frac{L}{R_t} = \frac{L}{3 \cdot (R_u + R_v + R_w)} = \frac{L}{3 \cdot R} \quad (3.40)$$

where  $R_t$  is total resistance of motor.

Therefore, the equation of the BLDC can now be obtained as follows:

$$G(s) = \frac{\dot{\phi}}{V_s} = \frac{\frac{1}{k_e}}{\tau_m \cdot \tau_e \cdot s^2 + \tau_m \cdot s + 1} \quad (3.41)$$

If the gear ratio  $N$  of the gear box is considered in modeling, Eq. (3.41) becomes:

$$G(s) = \frac{\dot{\phi}}{V_s} = \frac{\frac{N}{k_e (\tau_m \cdot \tau_e)}}{s^2 + (\tau_m / \tau_m \cdot \tau_e) \cdot s + (1 / \tau_m \cdot \tau_e)} \quad (3.42)$$

The state space of Eq. (3.42) is obtained using following steps.

$$G(s) = \frac{\dot{\phi}(s)}{V_s(s)} = \frac{b_0}{s^2 + a_1 \cdot s + a_0} \quad (3.43)$$

From Eq. (3.43), the followings are obtained.

$$\dot{\phi}(s) \cdot (s^2 + a_1 \cdot s + a_0) = V_s(s) \cdot b_0 \quad (3.44)$$

$$s^2 \dot{\phi}(s) = -a_1 s \dot{\phi}(s) - a_0 \dot{\phi}(s) + V(s) \cdot b_0 \quad (3.45)$$

Eq. (3.45) can be transformed in the time variable

$$\ddot{\varphi}(t) = -a_1\dot{\varphi}(t) - a_0\varphi(t) + b_0u(t) \quad (3.46)$$

Taking  $x_1 = \dot{\varphi}(t)$ ,  $x_2 = \ddot{\varphi}(t)$ ,  $u(t) = V_s(t)$ , and  $y = x_1$  the following are obtained.

$$\begin{aligned} \dot{x}_1 &= \ddot{\varphi}(t) = x_2 \\ \dot{x}_2 &= \ddot{\varphi}(t) = -a_1\dot{\varphi}(t) - a_0\varphi(t) + b_0u(t) = -a_1x_2 - a_0x_1 + b_0u \end{aligned} \quad (3.47)$$

Eq (3.47) can be expressed can be expressed in vector form as follows:

$$\begin{bmatrix} \dot{x}_1 \\ \dot{x}_2 \end{bmatrix} = \begin{bmatrix} 0 & 1 \\ -a_0 & -a_1 \end{bmatrix} \cdot \begin{bmatrix} x_1 \\ x_2 \end{bmatrix} + \begin{bmatrix} 0 \\ b_0 \end{bmatrix} \cdot u \quad \dot{\mathbf{x}} = \mathbf{Ax} + \mathbf{Bu} \quad (3.48)$$

$$y = \begin{bmatrix} 1 & 0 \end{bmatrix} \cdot \begin{bmatrix} x_1 \\ x_2 \end{bmatrix} \quad y = \mathbf{Cx} \quad (3.49)$$

where  $\begin{bmatrix} x_1 \\ x_2 \end{bmatrix} = \begin{bmatrix} \dot{\varphi} \\ \ddot{\varphi} \end{bmatrix}$ ,  $y = \dot{\varphi}$ ,  $a_0 = \frac{1}{\tau_m \cdot \tau_e}$ ,  $a_1 = \frac{1}{\tau_e}$  and  $b_0 = \frac{N}{k_e(\tau_m \cdot \tau_e)}$

where  $\mathbf{x}(t)$ :  $n$  order state vector,  $\mathbf{u}(t)$ :  $m$  order control input vector,  $\mathbf{y}(t)$ :  $p$  order output vector.

### 3.4. Velocity and orientation controller design

To control the velocity and orientation of AGV, optimal robust controller is applied for each wheel. The controller is separate for each wheel. The left wheel and right wheels are assumed to be identical. Therefore, in this section, controller design method for motor of right wheel is same to that of left wheel. The input of the motor is supply voltage  $V_s$  and the output is angular velocity of wheel  $\dot{\phi}$ .

The BLDC velocity output for wheel  $\dot{\phi} = y(t)$  is equal to reference ( $r \neq 0$ ) for  $t \rightarrow \infty$ , and does not become zero for  $t \rightarrow \infty$ . Furthermore, because  $u(t)$  has constant value for  $t \rightarrow \infty$ ,  $\lim_{t \rightarrow \infty} \dot{u}(t) = 0$ .

Thus, taking new control input  $\mathbf{v} = \dot{\mathbf{u}}(t)$  and considering disturbance in the Eqs. (3.48) ~ (3.49) can be rewritten as follows:

$$\dot{\mathbf{x}}_e(t) = \mathbf{A}_e \mathbf{x}_e + \mathbf{B}_e \mathbf{v} + \mathbf{D}_e \mathbf{d}(t) \quad (3.50)$$

$$y(t) = \mathbf{C}_e \mathbf{x}_e(t) \quad (3.51)$$

where  $\mathbf{d}(t)$  is unknown disturbance,

$$\mathbf{x}_e(t) = \begin{bmatrix} \mathbf{x}(t) \\ \mathbf{u}(t) \end{bmatrix}, \mathbf{A}_e = \begin{bmatrix} \mathbf{A} & \mathbf{B} \\ \mathbf{0} & \mathbf{0} \end{bmatrix}, \mathbf{B}_e = \begin{bmatrix} \mathbf{0} \\ \mathbf{I}_m \end{bmatrix}, \mathbf{C}_e = [\mathbf{C} \quad \mathbf{0}], \mathbf{D}_e = \begin{bmatrix} \mathbf{I}_m \\ \mathbf{0} \end{bmatrix}$$

In this thesis, the disturbance is assumed equal zero. For  $t \rightarrow \infty$ ,  $\dot{\mathbf{x}}_s = \lim_{t \rightarrow \infty} \dot{\mathbf{x}}(t) = 0$  and  $\mathbf{y}_s = \mathbf{C} \mathbf{x}_s = \lim_{t \rightarrow \infty} y(t) = r$ . And if  $\mathbf{x}(t)$  and  $\mathbf{u}(t)$  takes constant values  $\mathbf{x}_s$  and  $\mathbf{u}_s$ , respectively, this value is obtained from steady state solution of Eqs. (3.50) ~ (3.51).

$$\begin{bmatrix} \dot{\mathbf{x}}_s \\ \mathbf{y}_s \end{bmatrix} = \begin{bmatrix} \mathbf{0} \\ \mathbf{r} \end{bmatrix} = \begin{bmatrix} \mathbf{A} & \mathbf{B} \\ \mathbf{C} & \mathbf{0} \end{bmatrix} \begin{bmatrix} \mathbf{x}_s \\ \mathbf{u}_s \end{bmatrix} + \begin{bmatrix} \mathbf{d} \\ \mathbf{0} \end{bmatrix} \quad (3.52)$$

From Eq. (3.52), the following can be obtained.

$$\begin{bmatrix} \mathbf{x}_s \\ \mathbf{u}_s \end{bmatrix} = \begin{bmatrix} \mathbf{A} & \mathbf{B} \\ \mathbf{C} & \mathbf{0} \end{bmatrix}^{-1} \left( \begin{bmatrix} \mathbf{0} \\ \mathbf{r} \end{bmatrix} - \begin{bmatrix} \mathbf{d} \\ \mathbf{0} \end{bmatrix} \right) = \mathbf{Z}^{-1} \begin{bmatrix} -\mathbf{d} \\ \mathbf{r} \end{bmatrix} \quad (3.53)$$

Variation from steady state value  $\delta\mathbf{x}(t)$  and  $\delta\mathbf{u}(t)$  are as follows:

$$\begin{cases} \delta\mathbf{x}(t) = \mathbf{x}(t) - \mathbf{x}_s \\ \delta\mathbf{u}(t) = \mathbf{u}(t) - \mathbf{u}_s \end{cases} \quad (3.54)$$

Let  $\delta\mathbf{x}_e(t) = \begin{bmatrix} \delta\mathbf{x}(t) \\ \delta\mathbf{u}(t) \end{bmatrix}$ .

Using Eqs. (3.52) and (3.54), the followings are obtained as:

$$\delta\dot{\mathbf{x}}_e(t) = \begin{bmatrix} \delta\dot{\mathbf{x}}(t) \\ \delta\dot{\mathbf{u}}(t) \end{bmatrix} = \begin{bmatrix} \dot{\mathbf{x}}(t) - \dot{\mathbf{x}}_s \\ \delta\mathbf{v}(t) \end{bmatrix} = \begin{bmatrix} \mathbf{A} & \mathbf{B} \\ \mathbf{0} & \mathbf{0} \end{bmatrix} \begin{bmatrix} \delta\mathbf{x}(t) \\ \delta\mathbf{u}(t) \end{bmatrix} + \begin{bmatrix} \mathbf{0} \\ \mathbf{I}_m \end{bmatrix} \delta\mathbf{v}(t) \quad (3.55)$$

$$\mathbf{y} - \mathbf{y}_s = \mathbf{y} - \mathbf{r} = -\mathbf{y}_e(t) = \mathbf{C}(\mathbf{x} - \mathbf{x}_s) = \mathbf{C}\delta\mathbf{x}(t) = [\mathbf{C} \quad \mathbf{0}] \begin{bmatrix} \delta\mathbf{x}(t) \\ \delta\mathbf{u}(t) \end{bmatrix} = \mathbf{C}_e \mathbf{x}_e(t) \quad (3.56)$$

$$\delta\dot{\mathbf{x}}_e = \mathbf{A}_e \delta\mathbf{x}_e(t) + \mathbf{B}_e \delta\mathbf{v}(t) \quad (3.57)$$

$$\mathbf{y}(t) - \mathbf{r} = \mathbf{C}_e \delta\mathbf{x}_e(t) \quad (3.58)$$

The controllability matrix  $\mathbf{V}_e$  and observability matrix  $\mathbf{N}_e$  of Eqs. (3.50) ~ (3.51) are:

$$\mathbf{V}_e = [\mathbf{B}_e \quad \mathbf{A}_e \mathbf{B}_e \quad \mathbf{A}_e^2 \mathbf{B}_e \quad \dots \quad \mathbf{A}_e^{n+m-1} \mathbf{B}_e] \quad (5.59)$$

$$\mathbf{N}_e^T = \begin{bmatrix} \mathbf{C}_e \\ \mathbf{C}_e \mathbf{A}_e \\ \mathbf{C}_e \mathbf{A}_e^2 \\ \vdots \\ \mathbf{C}_e \mathbf{A}_e^{n+m-1} \end{bmatrix} \quad (5.60)$$

So if this system is controlled to be  $\delta \mathbf{x}_e(\mathbf{t}) \rightarrow 0$  as  $\mathbf{t} \rightarrow 0$ , it is known that  $\mathbf{y}(\mathbf{t}) \rightarrow \mathbf{r}$ . If  $(\mathbf{A}, \mathbf{B})$  is controllable,  $\text{rank}(\mathbf{V}_e) = n + m$ ,  $(\mathbf{A}_e, \mathbf{B}_e)$  is controllable. If  $(\mathbf{C}, \mathbf{A})$  is observable,  $\text{rank}(\mathbf{N}_e^T) = n + m$ . If  $\text{rank}(\mathbf{Z}) = n + m$ ,  $(\mathbf{C}_e, \mathbf{A}_e)$  is observable.

Using optimal regulator,  $\delta \mathbf{x}_e(\mathbf{t}) \rightarrow 0$  can be done. That is, cost function is defined as:

$$J_e = \int_0^{\infty} \left( \|\delta \mathbf{x}_e(\mathbf{t})\|_{\mathbf{Q}_e}^2 + \|\mathbf{v}(\mathbf{t})\|_{\mathbf{R}_e}^2 \right) dt \quad (3.61)$$

where  $\mathbf{Q}_e : (n + m) \times (n + m)$  semi-positive definite symmetric matrix,  
 $\mathbf{R}_e : m \times m$  symmetric matrix.

Minimizing this cost function, optimal regulator problem can be solved. And let  $\mathbf{Q}_e = \mathbf{C}_e^T \mathbf{C}_e$ . Cost function Eq. (3.61) is defined as:

$$J_e = \int_0^{\infty} \left( \|\mathbf{y}(\mathbf{t}) - \mathbf{r}\|_{\mathbf{Q}_e}^2 + \|\mathbf{v}(\mathbf{t})\|_{\mathbf{R}_e}^2 \right) dt \quad (3.62)$$

The cost function is obtained by taking a weight to deviation of output and reference and control input. Solution of optimal regulator that minimizing Eq. (3.61) is

$$\mathbf{v}(\mathbf{t}) = -\mathbf{F}_e \delta \mathbf{x}_e(\mathbf{t}) \quad (3.63)$$

where

$$\mathbf{F}_e = \mathbf{R}_e^{-1} \mathbf{B}_e \mathbf{P}_e \quad (3.64)$$

$\mathbf{P}_e : (n+m) \times (n+m)$  is positive definite matrix and solution of the following Riccati Equation:

$$\mathbf{A}_e^T \mathbf{P}_e + \mathbf{P}_e \mathbf{A}_e + \mathbf{Q}_e - \mathbf{P}_e \mathbf{B}_e^{-1} \mathbf{R}_e^{-1} \mathbf{B}_e^T \mathbf{P}_e = \mathbf{0} \quad (3.65)$$

Transforming this into type of feedback state  $\mathbf{x}(\mathbf{t})$  and deviation  $\mathbf{y}_e(\mathbf{t}) \rightarrow \mathbf{r} - \mathbf{y}(\mathbf{t})$  yields as follows:

Substituting Eq. (3.54) into Eq. (3.62), can be written as follows:

$$\mathbf{v}(\mathbf{t}) = -\mathbf{F}_e \begin{bmatrix} \mathbf{x}(\mathbf{t}) \\ \mathbf{u}(\mathbf{t}) \end{bmatrix} + \mathbf{F}_e \begin{bmatrix} \mathbf{x}_s \\ \mathbf{u}_s \end{bmatrix} \quad (3.66)$$

Eqs. (3.50) ~ (3.51) is expressed into matrix form as

$$\begin{bmatrix} \dot{\mathbf{x}}(t) \\ \mathbf{y}(t) \end{bmatrix} = \mathbf{Z} \begin{bmatrix} \mathbf{x}(t) \\ \mathbf{u}(t) \end{bmatrix} + \mathbf{F}_e \begin{bmatrix} \mathbf{d} \\ \mathbf{0} \end{bmatrix} \quad (3.67)$$

From Eq. (3.66), the following is obtained

$$\begin{bmatrix} \mathbf{x}(t) \\ \mathbf{u}(t) \end{bmatrix} = \mathbf{Z}^{-1} \begin{bmatrix} \dot{\mathbf{x}}(t) - \mathbf{d} \\ \mathbf{y}(t) \end{bmatrix} \quad (3.68)$$

Using Eq. (3.53) and Eq. (3.67), Eq. (3.62) is transformed into

$$\begin{aligned} \mathbf{v}(t) = \dot{\mathbf{u}}(t) &= -\mathbf{F}_e \begin{bmatrix} \mathbf{x}(t) \\ \mathbf{u}(t) \end{bmatrix} + \mathbf{F}_e \begin{bmatrix} \mathbf{x}_s \\ \mathbf{u}_s \end{bmatrix} = -\mathbf{F}_e \mathbf{Z}^{-1} \begin{bmatrix} \dot{\mathbf{x}}(t) - \mathbf{d} \\ \mathbf{y}(t) \end{bmatrix} + \mathbf{F}_e \mathbf{Z}^{-1} \begin{bmatrix} -\mathbf{d} \\ \mathbf{r} \end{bmatrix} \\ &= -\mathbf{F}_e \mathbf{Z}^{-1} \begin{bmatrix} \dot{\mathbf{x}}(t) \\ \mathbf{y}(t) - \mathbf{r} \end{bmatrix} = -\mathbf{K}_1 \dot{\mathbf{x}}(t) - \mathbf{K}_2 (\mathbf{y}(t) - \mathbf{r}) = -\mathbf{K}_1 \dot{\mathbf{x}}(t) + \mathbf{K}_2 \mathbf{y}_e(t) \end{aligned} \quad (3.69)$$

where

$$\mathbf{F}_e \mathbf{Z}^{-1} = \begin{bmatrix} \underbrace{\mathbf{K}_1}_n & \underbrace{\mathbf{K}_2}_{m=p} \end{bmatrix} \quad (3.70)$$

Integrating Eq. (3.69) from 0 to  $t$ , control law is obtained as follows:

$$\mathbf{u}(t) = -\mathbf{K}_1 \mathbf{x}(t) + \mathbf{K}_2 \int_0^t \mathbf{y}_e(\tau) d\tau + \mathbf{K}_1 \mathbf{x}(0) \quad (3.71)$$

In this thesis  $\mathbf{u}(t) = V_s$ ,  $\mathbf{x}(t) = [\dot{\phi} \quad \ddot{\phi}]$ , and  $y = \dot{\phi}$ .



## Chapter 4: Obstacle Avoidance Algorithm

This chapter describes the proposed obstacle avoidance algorithm. This algorithm consists of obstacle detector, moving object tracking based on Kalman filter, collision possibility prediction and obstacle avoidance policy.

### 4.1. Obstacle Detector

To detect the local environment, the laser measurement system LMS-151 is applied to AGV as shown in Fig. 4.1. This sensor scans the environment by transmitting and receiving the laser signal over desired area. The definition of this area  $W (R_s, \theta_{start}, \theta_{end})$  is given by  $R_s = 20$  m,  $\theta_{start} = 0^\circ$ ,  $\theta_{end} = 180^\circ$  where  $R_s$  is the radius of scanning area,  $\theta_{start}$  the start angle, and  $\theta_{end}$  the end angle. The resolution of laser scanning is  $0.5^\circ$  and scanning frequency is 25 Hz.

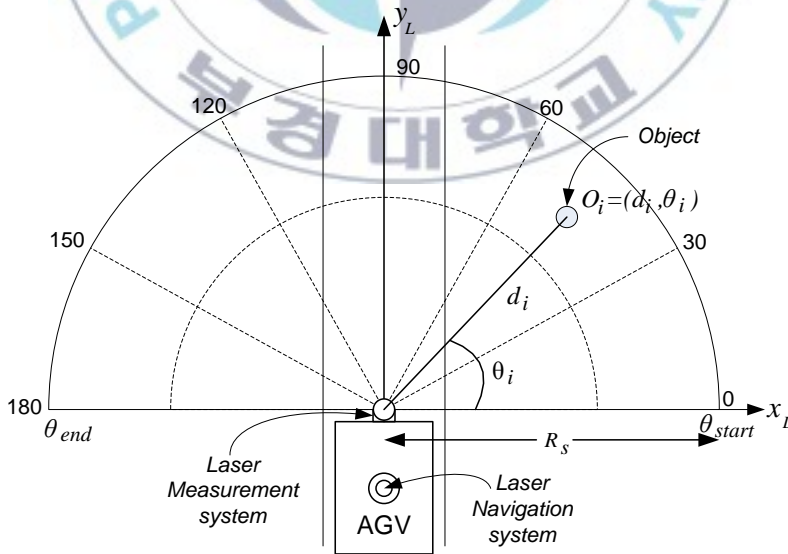


Fig. 4.1 LMS-151 scanning area

where  $y_L$  is the center of laser scanner,  $\theta_i$  is the angle between the object  $O_i$  and horizontal axis  $x_L$ . The detected object can be expressed with polar coordinate as  $(d_i, \theta_i)$ , or with Cartesian coordinates in local coordinate of LMS-151 as:

$$O_i = (O_{ixL}, O_{iyL}) = (d_i \cos \theta_i, d_i \sin \theta_i) \text{ for } i = 1, \dots, n \quad (4.1)$$

The positioning method using NAV-200 is shown in Fig. 4.2.

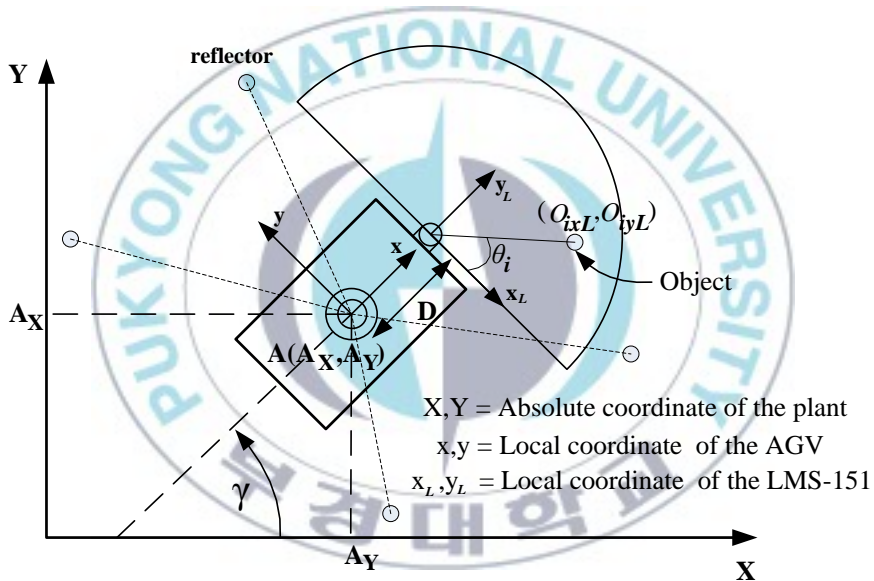


Fig. 4.2 Positioning using NAV-200

The reflector positions in absolute coordinate system of the plant are saved inside the AGV's memory. By comparing the reflector scanning result and the reflector coordinate in AGV's memory, the absolute coordinate and orientation of AGV are obtained.

Using coordinate transformation, the position of obstacle  $O_i$  in the global coordinate is obtained:

$$\begin{bmatrix} O_{ix} \\ O_{iy} \end{bmatrix} = \begin{bmatrix} A_x \\ A_y \end{bmatrix} + \begin{bmatrix} \cos \gamma & -\sin \gamma \\ \sin \gamma & \cos \gamma \end{bmatrix} \begin{bmatrix} O_{ixL} \\ O_{iyL} \end{bmatrix} + D \begin{bmatrix} \cos \gamma \\ \sin \gamma \end{bmatrix} \quad (4.2)$$

where  $A$  is the position of AGV in global coordinate,  $\gamma$  is orientation of AGV from X axis and  $D$  is distance between NAV-200 and LMS-151.

#### 4.2. Moving Object Tracking Based on Kalman Filter

In factory environment, the moving objects are mainly persons that their accelerations change slowly. Therefore, an uniform motion model can be set up with acceleration as white Gaussian noise. The state vector of the object is  $\mathbf{X} = [O_x \ V_{ox} \ O_y \ V_{oy}]^T$  and the observation vector is  $\mathbf{Y} = [O_x \ O_y]^T$  where  $O_x, O_y$  are position of the obstacle, and  $V_{ox}, V_{oy}$  are components of obstacle velocity  $V_o$  in directions of X, Y, respectively.

The state equation of moving object in discrete time system is given as follows:

$$\mathbf{X}(k) = \mathbf{A}\mathbf{X}(k-1) + \mathbf{W}(k-1) \quad (4.3)$$

and measurement equation is:

$$\mathbf{Y}(k) = \mathbf{C}\mathbf{X}(k) + \mathbf{V}(k) \quad (4.4)$$

where  $\mathbf{W}$  is Gaussian process noise and  $\mathbf{V}$  is Gaussian measurement noise.

The state parameters for dead reckoning can be given as:

$$\mathbf{A} = \begin{bmatrix} 1 & T & 0 & 0 \\ 0 & 1 & 0 & 0 \\ 0 & 0 & 1 & T \\ 0 & 0 & 0 & 1 \end{bmatrix}, \mathbf{C} = \begin{bmatrix} 0 & 1 & 0 & 0 \\ 0 & 0 & 0 & 1 \end{bmatrix} \quad (4.5)$$

where  $T$  is observation period.

For the human motion, the covariance matrix of process noise can be determined by the following [8]:

$$\mathbf{W}(k) = \begin{bmatrix} \frac{T^3}{3} & \frac{T^2}{2} & 0 & 0 \\ \frac{T^2}{2} & T & 0 & 0 \\ 0 & 0 & \frac{T^3}{3} & \frac{T^2}{2} \\ 0 & 0 & \frac{T^2}{2} & T \end{bmatrix} \times a \quad (4.6)$$

where  $a$  is a factor determined by acceleration.

The covariance matrix of direct observation is:

$$\mathbf{V}(k) = \begin{bmatrix} \sigma_p^2 & 0 \\ 0 & \sigma_\theta^2 \end{bmatrix} \quad (4.7)$$

From the Kalman filter equations, the next step motion state of object can be estimated using prediction and update laws as follows:

Prediction:

$$\hat{X}(k | k-1) = A(k-1)X(k-1 | k-1) \quad (4.8)$$

$$P(k | k-1) = A(k-1)P(k-1 | k-1)A^T(k-1) + Q(k-1) \quad (4.9)$$

Update:

$$\hat{X}(k | k) = \hat{X}(k | k-1) + K(k)[Z(k) - C(k)\hat{X}(k | k-1)] \quad (4.10)$$

$$K(k) = P(k | k-1)C^T(k)[C(k)P(k | k-1)C^T(k) + R(k)]^{-1} \quad (4.11)$$

$$P(k | k) = [I - K(k)C(k)]P(k | k-1) \quad (4.12)$$

### 4.3. Collision Possibility Prediction

Based on the obstacle movement prediction by Kalman filter, the collision possibility is predicted. When the AGV velocity is  $V_A$ , and the predicted obstacle velocity is  $\hat{V}_O$ , the relative velocity between the obstacle and the AGV is:

$$V_{OA} = \hat{V}_O - V_A \quad (4.13)$$

The collision condition is estimated by projecting the obstacle to the AGV dimension. To simplify the calculation, only the edges of obstacle and the nearest point from the obstacle to AGV are calculated.

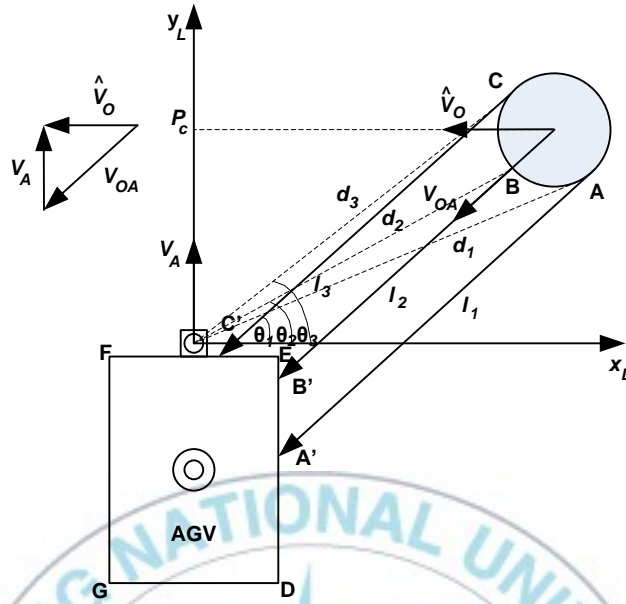


Fig. 4.3 Obstacle projection

The obstacle line projection ( $l_1, l_2, l_3$ ) equation is obtained by:

$$y = m(x - O_{ixL}) + O_{iyL} \quad (4.14)$$

where  $m$  is gradient of the projection line,  $O_{ixL}$  is position in the  $x_L$  direction of obstacle and  $O_{iyL}$  is position in the  $y_L$  direction of obstacle in their direction. Because the gradient of projection line is similar with the direction of the obstacle,  $m$  is denote by  $m = \frac{V_{OAy}}{V_{OAx}}$ .

Position in the  $x_L$  axis is denoted by  $O_{ixL} = d_i \cos \theta_i$  and position in  $y_L$  axis is denoted by  $O_{iyL} = d_i \sin \theta_i$  for  $i = 1, 2, 3, \dots$ .

The hit points A', B' and C' can be calculated as in Appendix A. If one of three line projections is intersected with one of AGV dimension line (DE, EF, FG, GD), the collision possibility is high.

The shortest distance between AGV and obstacle is:

$$l_{\min} = \min(l_1, l_2, l_3) \quad (4.15)$$

The anticipated collision time is:

$$t_c = \frac{l_{\min}}{|V_{OA}|} \quad (4.16)$$

and anticipated collision position is:

$$P_c = (V_{Ax} \cdot t_c, V_{Ay} \cdot t_c) \quad (4.17)$$

#### 4.4. Obstacle Avoidance Policy

Based on the collision possibility calculation, the obstacle avoidance policy is generated. To avoid the obstacle and find the shortest path to the goal, the tangent bug algorithm is applied. This algorithm is suitable for AGV using laser measurement system and also it guarantees the AGV so as to reach the goal position. Only based on the start position and goal position information, the AGV can find the path and avoid the obstacles efficiently. In Fig. 5, when the AGV finds the stationary obstacle, the algorithm calculates the distance between the point  $O_i$  and  $q_{goal}$ . The AGV then goes to the shortest distance to get the optimal path.

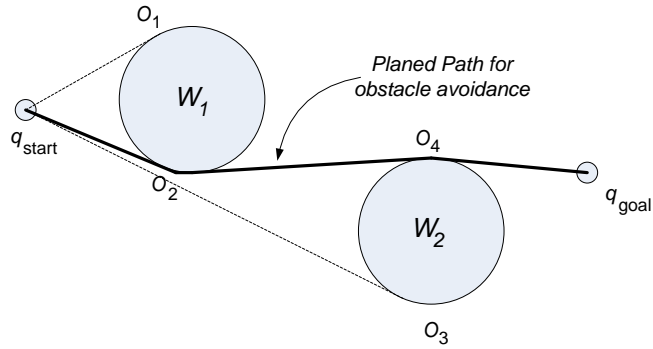


Fig. 4.4 Tangent Bug algorithm

When the moving obstacle is detected, the AGV reduces or increases the velocity depend on the velocity of obstacle. The increasing velocity policy is adopted if the following condition.

$$(V_{A_{\max}} - V_{A_{\text{now}}}) t_c > AC + \Delta L \quad (4.18)$$

where  $V_{A_{\max}}$  is AGV's maximum velocity,  $V_{A_{\text{now}}}$  is AGV's current velocity,  $t_c$  is anticipated collision time,  $AC$  is obstacle size, and  $\Delta L$  is save distance. When this condition is not satisfied, the AGV stops to avoid the collision condition.

## Chapter 5: Simulation and Experimental Results

To verify the effectiveness of the proposed velocity and orientation controller and obstacle avoidance algorithm, simulation and experiment are done. Simulation and experiment for proposed velocity and orientation are done using desired velocity and orientation. Simulation and experiment for proposed obstacle avoidance algorithm are done using stationary and moving obstacle.

The configuration and parameters of the AGV for simulation and experiment are shown in Fig. 5.1. and Table 5.1 as follows:

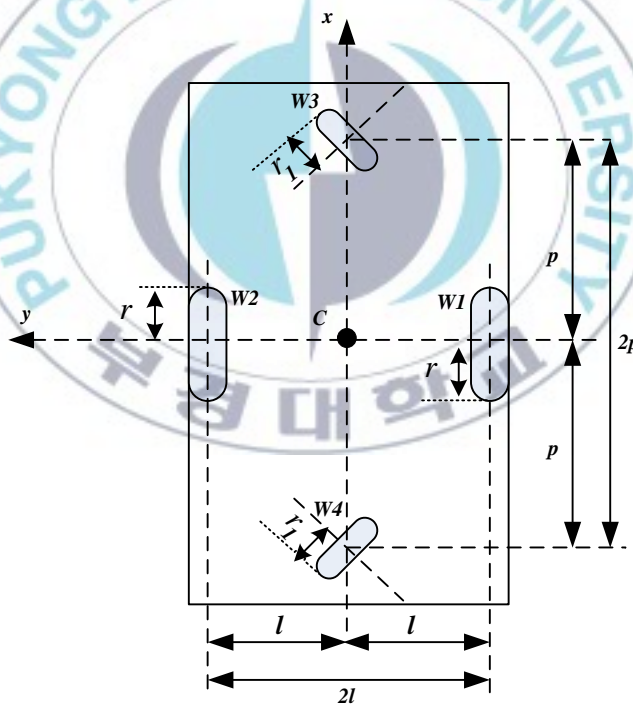


Fig. 5.1 Configuration of AGV

Table 5.1 Parameters of AGV

Parameter	Values	Units
Radius of driving wheel ( $r$ )	0.075	[m]
Radius of castor wheel ( $r_i$ )	0.04	[m]
Right and left wheel to center distance ( $l$ )	0.30	[m]
Front and back wheel to center distance ( $p$ )	0.40	[m]

The parameters of BLDC motor used in this thesis is shown in Table 5.2.

Table 5.2. Parameters of BLDC motor

No	Parameter	Rating
1	Rated Voltage	24 V
2	Rated Output	200 W
3	Rated Current	11.9 A
4	Rated Speed	3000 RPM
5	Rated Torque	6.3 Kgf-cm
6	Weight	2.7 Kg
7	Voltage constant ( $k_e$ )	14.8 V/Krpm
8	Torque Constant ( $k_t$ )	1.4 kgf.cm = 0.137 Nm
9	Rotor inertia ( $J$ )	$0.24 \times 10^{-3} \text{ kg.m}^2$
10	Armature resistance ( $R$ )	0.9 ohm
11	Armature inductance ( $L$ )	0.9 mH
12	Mechanical time constant ( $\tau_m$ )	10 ms
13	Electrical time constant ( $\tau_e$ )	1.1ms
14	Gear ratio ( $N$ )	1/24

## 5.1. Simulation result

### 5.1.1. Velocity and orientation controller

To design the velocity and orientation controller, the transfer function of BLDC motor described by:

$$G(s) = \frac{\omega_m(s)}{V_s(s)} = \frac{b_0}{s^2 + a_1 \cdot s + a_0}$$

where

$$a_0 = \frac{1}{\tau_m \cdot \tau_e}, \quad a_1 = \frac{1}{\tau_e}, \quad \text{and} \quad b_0 = \frac{N}{k_e(\tau_m \cdot \tau_e)}$$

So values for  $N$ ,  $k_e$ ,  $\tau_m$ , and  $\tau_e$  need to be calculated to obtain the motor model. From Table 5.1, the value of gear ratio  $N$  is 1/24, the value of mechanical time constant  $\tau_m$  is 10 ms, the value of electrical time constant  $\tau_e$  is 1.1 ms, and the voltage constant  $k_e$  is 14.8 V/Krpm.

Therefore, the value of BLDC parameter can be calculated as:

$$a_0 = \frac{1}{\tau_m \cdot \tau_e} = \frac{1}{1 \cdot 10^{-2} \cdot 1.1 \cdot 10^{-3}} = 90909$$

$$a_1 = \frac{1}{\tau_e} = \frac{1}{1.1 \cdot 10^{-3}} = 909$$

$$b_0 = \frac{N}{k_e(\tau_m \cdot \tau_e)} = \frac{\frac{1}{24}}{0.0148 \cdot (1 \cdot 10^{-2} \cdot 1.1 \cdot 10^{-3})} = 255937$$

The transfer function of BLDC motor is:

$$G(s) = \frac{\omega_m(s)}{V_s(s)} = \frac{255937}{s^2 + 909 \cdot s + 90909}$$

Using Eqs. (3.48) ~ (3.49), the state equation of BLDC motor is:

$$\begin{bmatrix} \dot{x}_1 \\ \dot{x}_2 \end{bmatrix} = \begin{bmatrix} 0 & 1 \\ -a_0 & -a_1 \end{bmatrix} \cdot \begin{bmatrix} x_1 \\ x_2 \end{bmatrix} + \begin{bmatrix} 0 \\ b_0 \end{bmatrix} \cdot u \quad \dot{\mathbf{x}} = \mathbf{Ax} + \mathbf{Bu}$$

$$y = \begin{bmatrix} 1 & 0 \end{bmatrix} \cdot \begin{bmatrix} x_1 \\ x_2 \end{bmatrix} \quad y = \mathbf{Cx}$$

$$\mathbf{A} = \begin{bmatrix} 0 & 1 \\ -90909 & -909 \end{bmatrix}, \quad \mathbf{B} = \begin{bmatrix} 0 \\ 255937 \end{bmatrix}, \quad \mathbf{C} = \begin{bmatrix} 1 & 0 \end{bmatrix}$$

To calculate controller gain, firstly matrix  $\mathbf{Z}$  is considered as follows:

$$\mathbf{Z} = \begin{bmatrix} \mathbf{A} & \mathbf{B} \\ \mathbf{C} & \mathbf{0} \end{bmatrix} = \begin{bmatrix} 0 & 1 & 0 \\ -90909 & -909 & 255937 \\ 1 & 0 & 0 \end{bmatrix}$$

where matrix  $\mathbf{Z}$  is full rank.

Secondly, state and output equation are obtained as follows:

$$\dot{\mathbf{x}}_e(\mathbf{t}) = \mathbf{Ax}_e + \mathbf{B}_e \mathbf{v} + \mathbf{D}_e \mathbf{d}(\mathbf{t})$$

$$\mathbf{y}(\mathbf{t}) = \mathbf{C}_e \mathbf{x}_e(\mathbf{t})$$

where,

$$\mathbf{x}_e(t) = \begin{bmatrix} \mathbf{x}(t) \\ \mathbf{u}(t) \end{bmatrix}, \quad \mathbf{A}_e = \begin{bmatrix} \mathbf{A} & \mathbf{B} \\ \mathbf{0} & \mathbf{0} \end{bmatrix} = \begin{bmatrix} 0 & 1 & 0 \\ -90909 & -909 & 255937 \\ 0 & 0 & 0 \end{bmatrix},$$

$$\mathbf{B}_e = \begin{bmatrix} \mathbf{0} \\ \mathbf{I}_m \end{bmatrix} = \begin{bmatrix} 0 \\ 0 \\ 1 \end{bmatrix}, \quad \mathbf{C}_e = [\mathbf{C} \quad \mathbf{0}] = [1 \quad 0 \quad 0], \quad \text{and} \quad \mathbf{D}_e = \begin{bmatrix} \mathbf{I}_m \\ \mathbf{0} \end{bmatrix} = \begin{bmatrix} 1 \\ 0 \\ 0 \end{bmatrix}$$

In this thesis, the disturbance  $\mathbf{d}(t)$  is assumed to be zero.

Thirdly, the value of  $\mathbf{Q}_e$  and  $\mathbf{R}_e$  are chosen as

$$\mathbf{Q}_e = \begin{bmatrix} 2 & 0 & 0 \\ 0 & 0 & 0 \\ 0 & 0 & 0 \end{bmatrix} \quad \text{and} \quad \mathbf{R}_e = 1000$$

Then from Riccati equation, solution  $\mathbf{P}_e$  is obtained as follows:

$$\mathbf{P}_e = \begin{bmatrix} 0.0111 & 1.1 \cdot 10^{-5} & 2.5049 \cdot 10^{-5} \\ 1.1 \cdot 10^{-5} & 1.2101 \cdot 10^{-8} & 3.0963 \cdot 10^{-8} \\ 2.5049 \cdot 10^{-5} & 3.0963 \cdot 10^{-8} & 0.004 \end{bmatrix}$$

Optimal feedback gain  $\mathbf{F}_e$  can be obtained by solving Eq. (3.64)

$$\mathbf{F}_e = \mathbf{R}_e^{-1} \mathbf{B}_e^T \mathbf{P}_e$$

$$\mathbf{F}_e = \begin{bmatrix} \underbrace{9.8919 \quad 0.0109}_{K1} & \underbrace{1000}_{K2} \end{bmatrix}$$

The proposed gain then is applied to the left and right wheel motors to control the angular velocity  $\dot{\phi}_R$  and  $\dot{\phi}_L$  of each wheel. The simulation result of control input for left and right wheels are shown in Fig. 5.2 as follows. Fig. 5.2 shows that the input control of the left and right AGV wheels at  $t=0s$  until  $t=2s$  is increased from  $0V$  to  $2.8V$  when the AGV accelerate. At  $t=4.5s$  until  $t=8s$ , the right wheel voltage is increased until  $3.9V$  and the left wheel voltage is decreased until  $1.8V$ . At this condition, the AGV is turned to the left direction. At  $t=8s$  until  $t=12s$ , the AGV keeps the orientation constant. Therefore, the voltages for left and right wheels are  $2.8V$ . At  $t=12s$  until  $t=14.5s$ , the left wheel voltage is decreased until  $1.8V$  and right wheel is increased until  $3.9V$ . At this condition, the AGV is turned right. At  $t=18s$  until  $t=20s$ , the left and right wheel voltages are decreased from  $2.8V$  to  $0V$ .

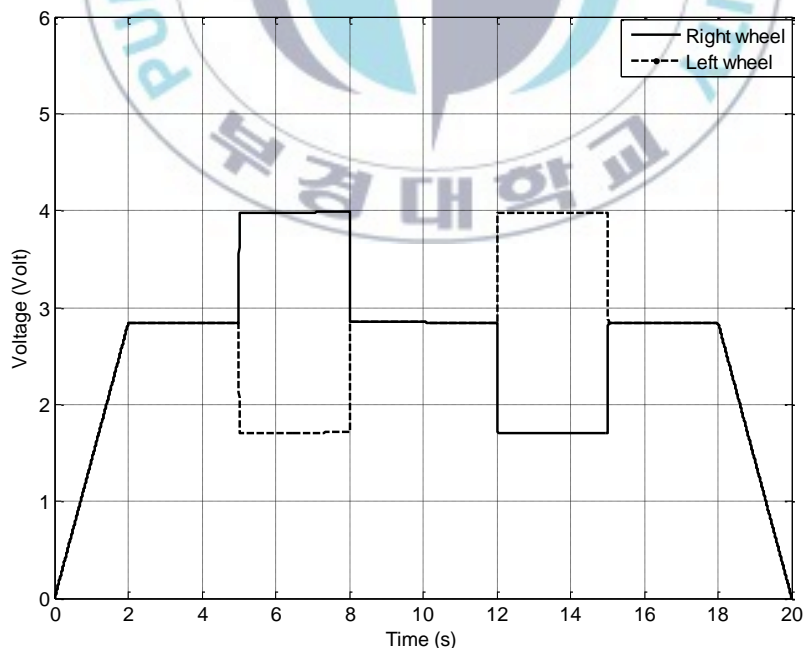


Fig. 5.2 Control input voltages for left and right wheels

Fig. 5.3 and Fig. 5.4 show the simulation result of linear velocity and orientation of AGV. The output velocity and orientation of AGV are similar with the reference signals. Fig. 5.3 shows that the linear velocity of AGV follows the reference signal. The AGV is accelerated from 0 to 0.25 m/s in 2s and keeps the constant value at 0.25 m/s even when the AGV turns left at  $t=4.5s$  until  $t=8s$  and turns right at  $t=12s$  until  $t=14.5s$  as shown in Fig. 5.4. At  $t=18s$  until  $t=20s$ , the AGV reduces the linear velocity gradually until it stops. The linear velocity error in Fig. 5.5 is bounded around  $\pm 2.4 \times 10^{-4} m/s$ . In Fig. 5.6, the orientation error is bounded around  $\pm 5.8 \times 10^{-4} rad$ .

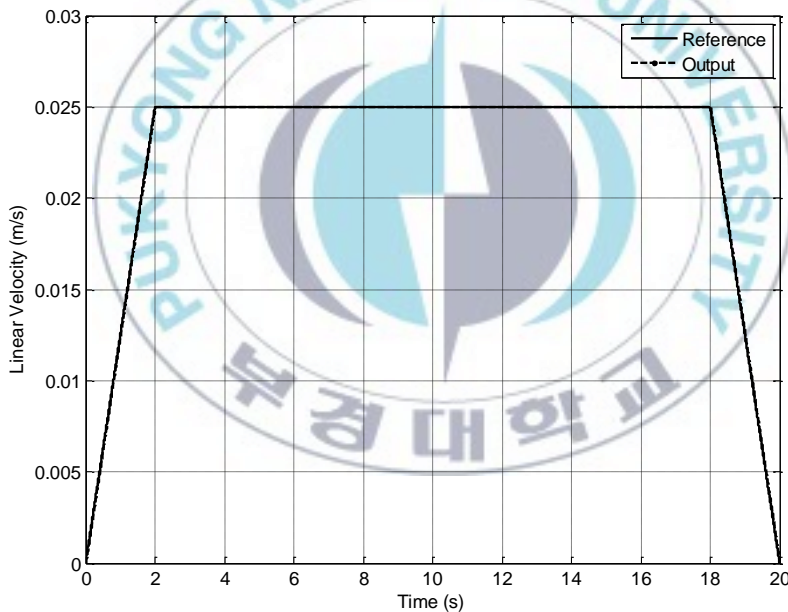


Fig. 5.3 Output of linear velocity

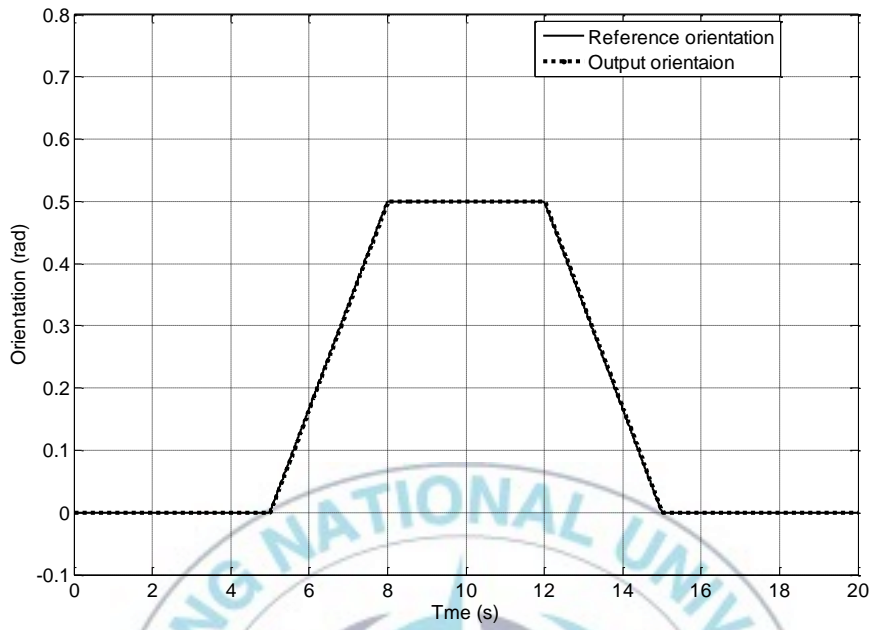


Fig. 5.4 Output of orientation

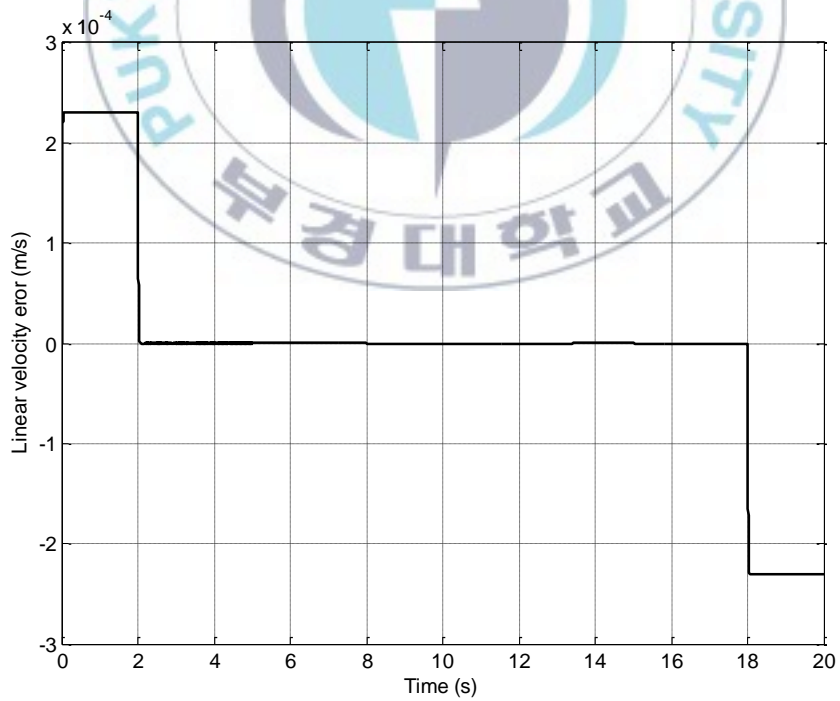


Fig. 5.5 Linear velocity error

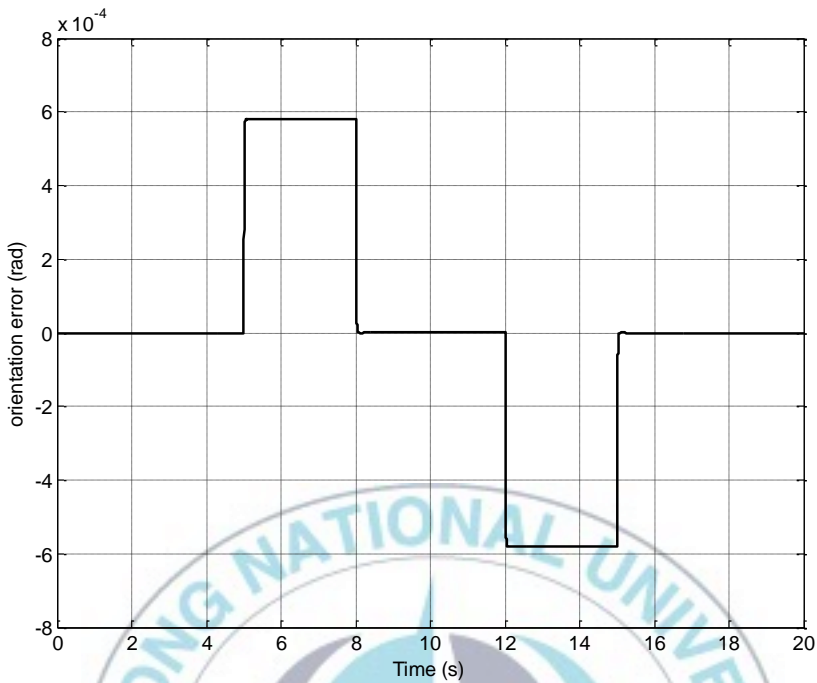


Fig. 5.6 Orientation error

### 5.1.2. Obstacle avoidance algorithm

The simulation environment of obstacle avoidance using stationary obstacle and moving obstacle is shown in Fig. 5.7.

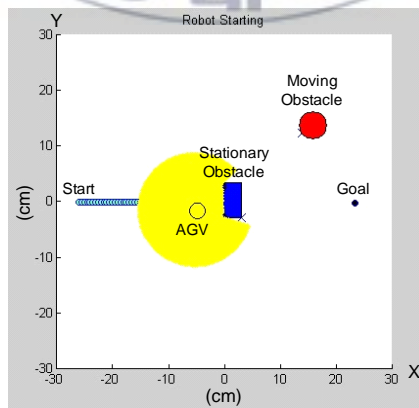


Fig. 5.7 Simulation environment

Fig. 5.8 shows the simulation result of obstacle avoidance with 2 stationary obstacles.

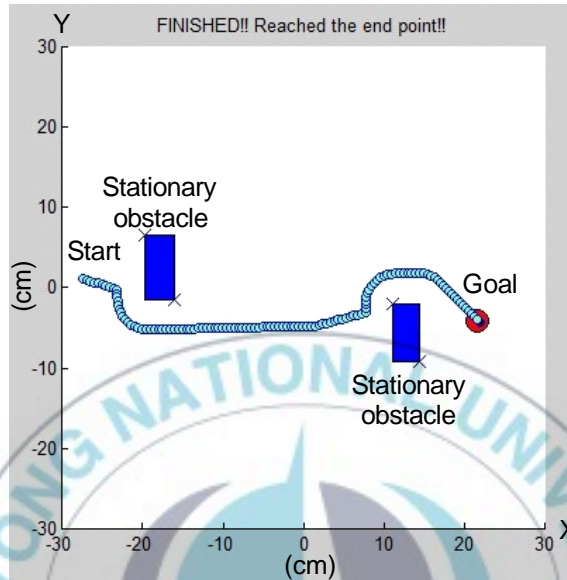


Fig. 5.8 Simulation results for stationary obstacle

Fig. 5.8 shows two rectangular shape stationary obstacles are placed in coordinate  $(-18, 3)$  and  $(12, -8)$ . The start point is  $(-28, 2)$  and the goal point is  $(21, -4)$ . The AGV moves with given constant velocity  $0.25\text{m/s}$  from start toward goal. The prediction obstacle velocity using Kalman filter is 0. Therefore, tangent bug algorithm is used for avoiding the obstacle. Fig. 5.8 shows that the AGV can reach the goal point.

Fig. 5.9 shows the result for moving obstacle with transversal direction.

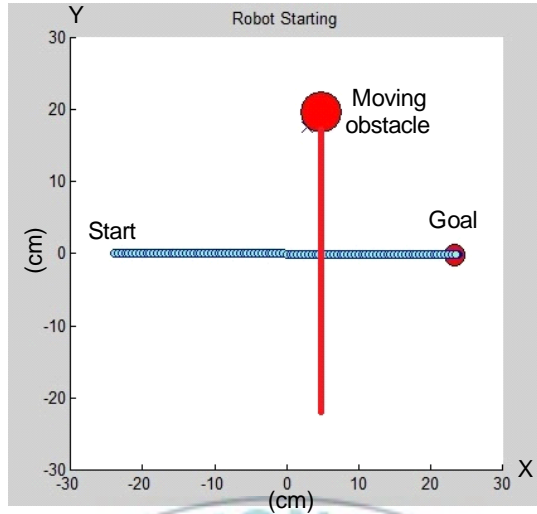


Fig. 5.9 Simulation results for moving obstacle with transversal direction

The AGV moves from start position at  $(-25, 0)$  to the goal position at  $(24, 0)$  with linear velocity of  $0.25\text{m/s}$ . Based on the Kalman filter motion prediction, the moving obstacle in transversal direction moves with prediction velocity  $0.3\text{m/s}$ . The trajectories of AGV and obstacle are shown in Fig. 5.9.

Fig. 5.10 shows the simulation result for moving obstacle with longitudinal direction.

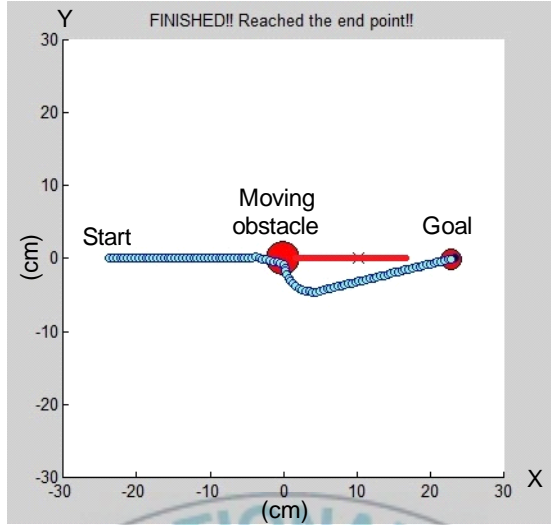


Fig. 5.10 Simulation results for moving obstacle with longitudinal direction

The AGV moves from start position at  $(-25, 0)$  to the goal position at  $(24, 0)$  with linear velocity of  $0.25\text{m/s}$ . Based on the Kalman filter motion prediction, the moving obstacle in longitudinal direction moves with prediction velocity  $0.3\text{m/s}$ . The trajectories of AGV and obstacle are shown in Fig. 5.10.

## 5.2. Experimental Results

### 5.2.1. Velocity and orientation controller

Figs. 5.11-5.15 show the experimental result of proposed velocity and orientation controller. Fig. 5.11 shows the control input voltages for left and right wheels. Fig. 5.12 shows that the linear velocity of AGV is following the simulation result. Fig. 5.13 shows orientation of AGV. Experimental result is following simulation result well. The linear velocity error in Fig. 5.14 is bounded around

$\pm 5 \times 10^{-2}$  m/s. Fig. 5.15 shows that the orientation error of AGV is bounded around  $\pm 0.1$  rad.

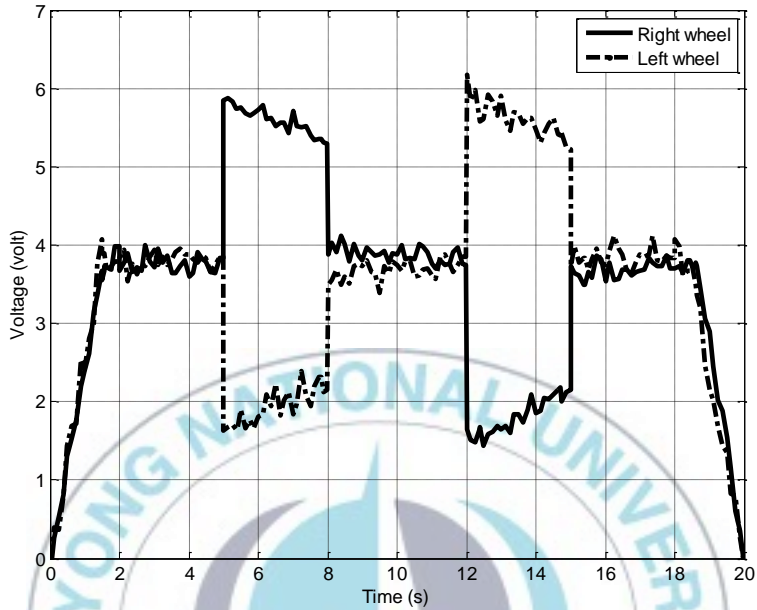


Fig. 5.11 Control input voltages for left and right wheels

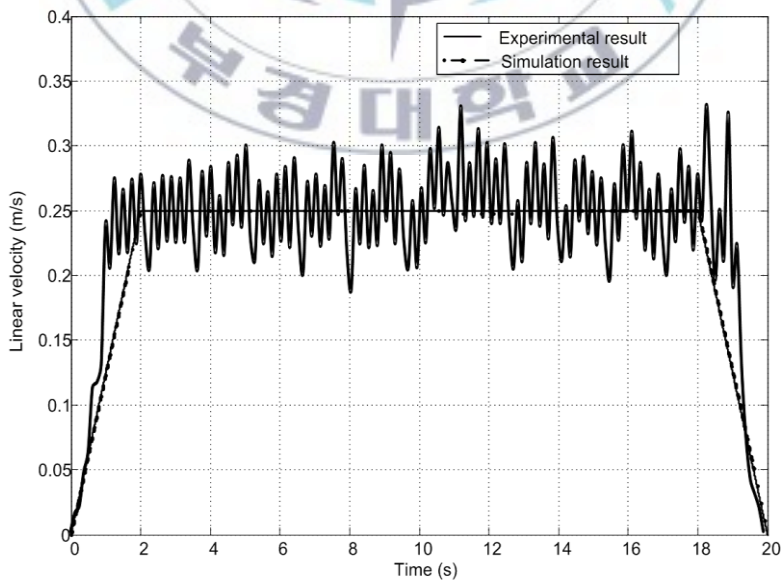


Fig. 5.12 Linear velocity of AGV

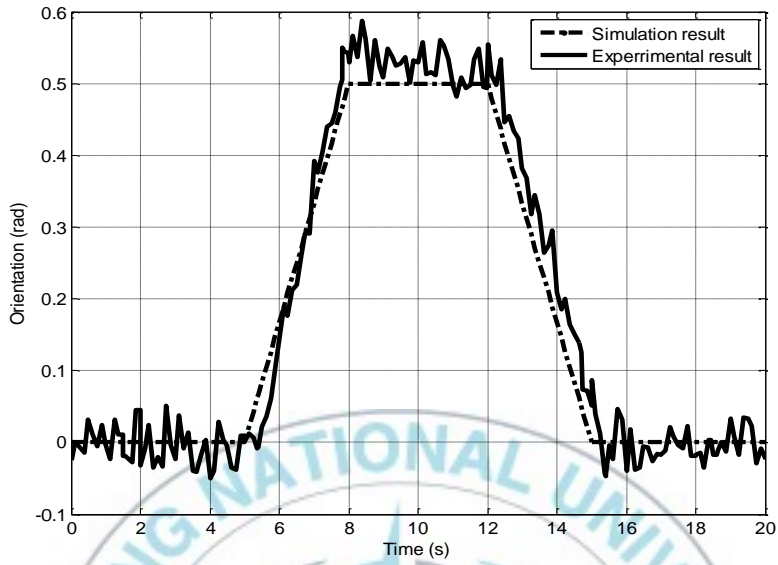


Fig. 5.13 Orientation of AGV

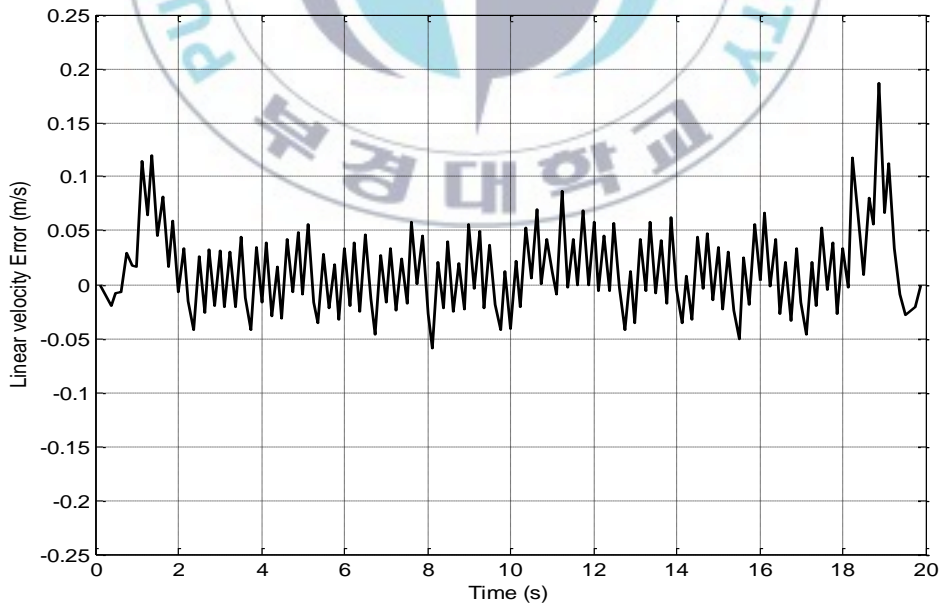


Fig. 5.14 Linear velocity error

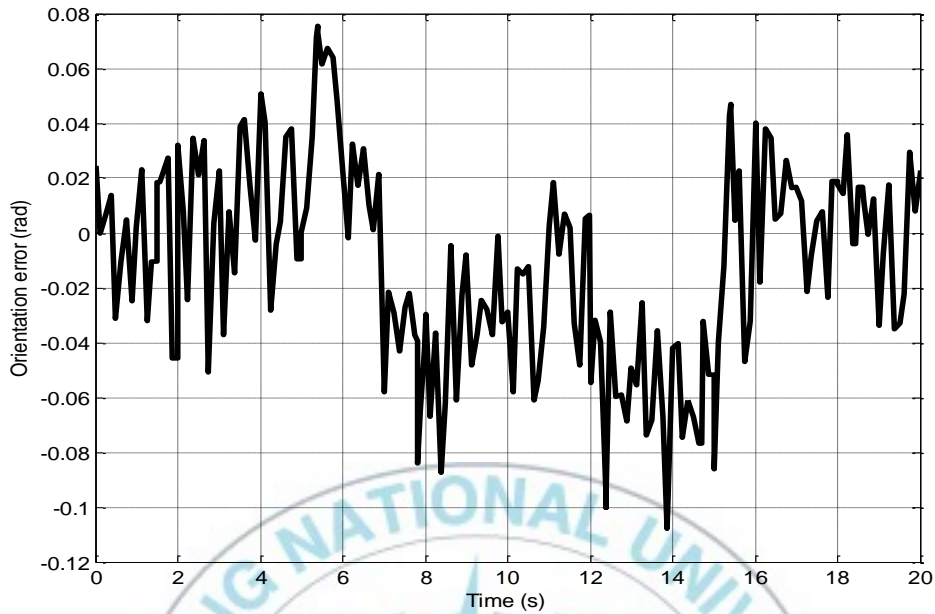


Fig. 5.15 Orientation error

## 5.2.2. Obstacle avoidance algorithm

### 5.2.2.1 Experimental result using 2 static obstacles.

The stationary obstacle experiment is shown in Fig. 5.16. Fig. 5.16(a) shows that the AGV detects the obstacle and predict the velocity of obstacle. The prediction result is 0m/s using Kalman filter. Therefore, based on tangent bug algorithm, the next point is decided. In Fig. 5.16(b), the AGV goes to the next shortest point toward goal. In Fig. 5.16(c), the AGV passes the obstacle and goes to the goal position. The trajectories of AGV from simulation and experiment are shown in Fig. 5.17. Experimental result is following simulation result well.

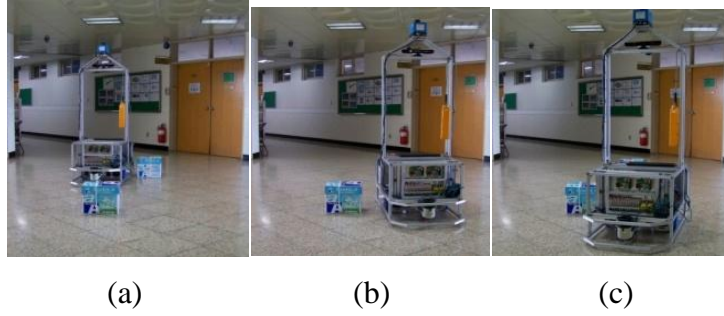


Fig. 5.16 Stationary obstacle avoidance

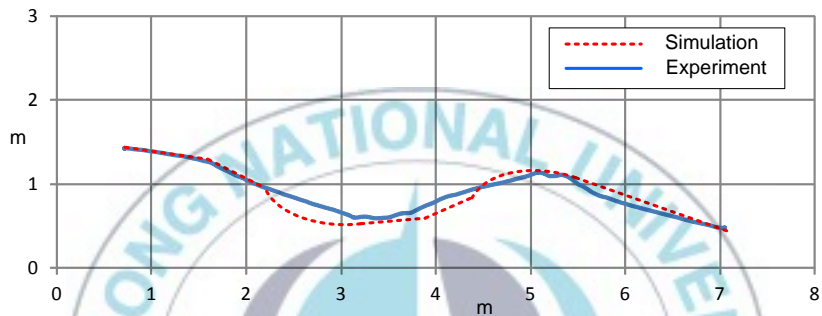


Fig. 5.17 Simulation and experiment trajectories for stationary obstacle avoidance

### 5.2.2.2 Experimental result using moving obstacle with transversal direction.

Fig. 5.18 shows the moving obstacle experiment in transversal direction. Fig. 5.18 (a) shows the Kalman filter predicts the obstacle velocity and decides the avoidance maneuver when the obstacle approaches. The predicted obstacle velocity using Kalman filter is bigger than maximum velocity of AGV. Therefore, the AGV decides to stop until the obstacle disappears as in shown Fig. 5.18 (b). Then AGV is moving continuously to goal position as shown in Fig. 5.18 (c). The trajectories of AGV from simulation and experiment are

shown in Fig. 5.19. Experimental result is following simulation result well.

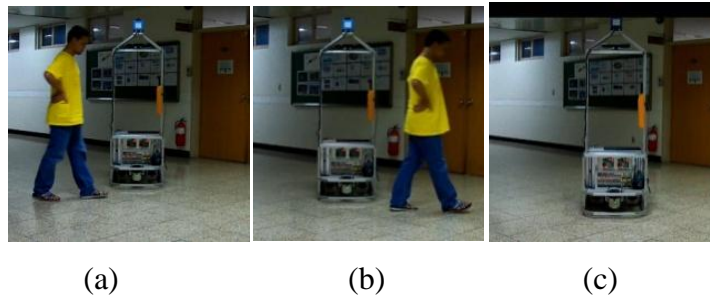


Fig. 5.18 Moving obstacle avoidance in transversal direction

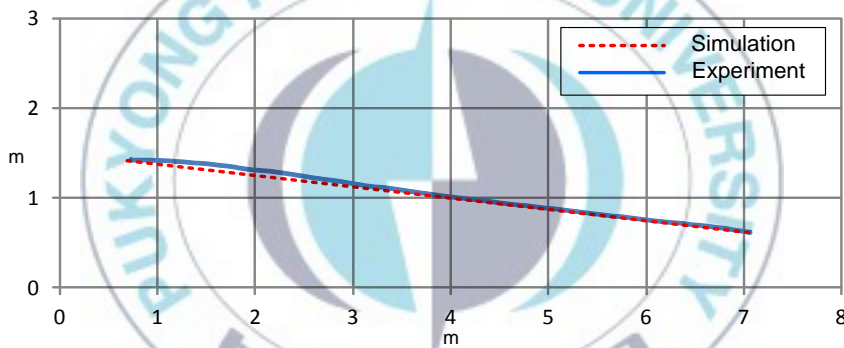


Fig. 5.19 Simulation and experiment trajectories for moving obstacle in transversal direction

### 5.2.2.3 Experimental result using moving obstacle with longitudinal direction

Fig. 5.20 shows the moving obstacle experiment in longitudinal direction. Fig. 5.20(a) shows the algorithm calculates the obstacle velocity based on Kalman filter and decides the avoidance maneuver when the obstacle approaches to the front of AGV. The algorithm decides to avoid the obstacle as in Fig. 5.20(b). Then AGV

is moving continuously to goal position as in Fig. 5.20(c). The trajectories of AGV from simulation and experiment are shown in Fig. 5.17. Experimental result is following simulation result well.

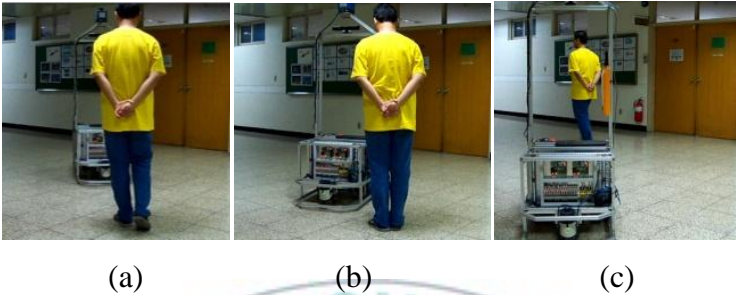


Fig. 5.20 Moving obstacle avoidance in longitudinal direction

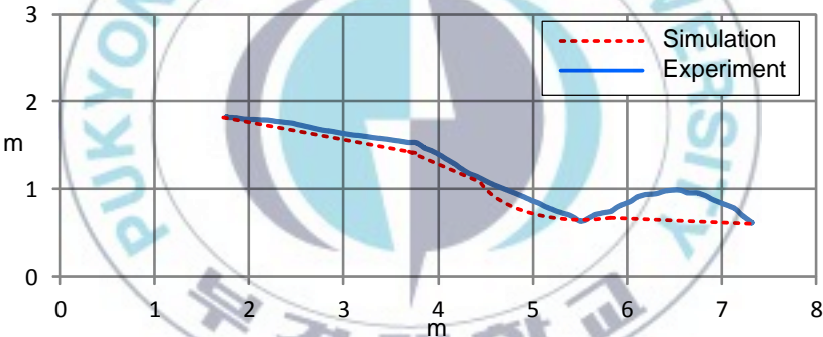


Fig. 5.21 Simulation and experiment trajectories for moving obstacle in longitudinal direction

## Chapter 6: Conclusions

### 6.1. Conclusion

This thesis propose an obstacle avoidance algorithm based on velocity and orientation controller for differential drive Automatic Guided Vehicles (AGV) system to avoid the stationary and moving obstacle in industrial environment. The conclusions of this thesis are summarized as follows:

- AGV's modeling including kinematic model of differential drive system is considered. Based on the sliding constraint and rolling constraint of fixed standard driving wheels and castor wheels, the kinematic modeling of differential drive AGV is obtained. Mathematic modeling of BLDC motor used for rotating driving wheels are given for simulation and controller design. Linear velocity control and orientation control are proposed based on optimal robust control theory.
- Obstacle avoidance algorithm is proposed to detect the environment quickly and reasonably to avoid the stationary and moving obstacles in factory environment for differential drive AGV system. The Cartesian coordinate of obstacle in absolute coordinate system is obtained from laser scanner LMS-151 measurement data. The Kalman filter based object tracking method was considered for the prediction of the AGV and obstacle velocity, which can improves the accuracy and obstacle avoidance ability. Based on object tracking algorithm, the collision possibility, collision time and position were

estimated. Finally, based on the obstacle avoiding policy, the orientation and velocity of AGV is calculated.

- Hardware design consists of mechanical design and electrical design. For mechanical design, AGV has two driving wheels on the left and right side, and two castor wheel in front and back side of AGV. For electrical design, AGV consists of sensors, controller, actuator and power supply. The sensors consist of laser measurement system and laser navigation system. The measurement system is used for obstacle detection and laser navigation system is used for positioning. The controller consists of industrial PC, touch screen monitor, wireless keyboard and wireless mouse. The actuators consist of motor driver and 2 BLDC motors. As power supply, 2x12V 80Ah batteries are employed in the AGV system.
- A software program are developed using C# programming language of visual studio 2008. This program collects all information from the laser measurement system through Ethernet (TCP/IP) communication and laser navigation system through serial communication (RS-232). Based on the given obstacle avoidance algorithm, the program controls the orientation and velocity of AGV based on optimal controller.
- The simulation and experiment results of linear velocity and orientation of AGV show that the AGV can follow the reference signals well. The AGV moves with constant velocity 0.25 m/s and can be accelerated and stop within 2 seconds. Furthermore, the linear velocity error is bounded around  $\pm 2.4 \times 10^{-4}$  m/s. The orientation error is bounded around  $\pm 5.8 \times 10^{-4}$  rad. The experimental results show that the AGV

successfully follows the reference signals that velocity error is bounded around  $\pm 5 \times 10^{-2}$  m/s and the orientation error is bounded around  $\pm 0.1$  rad.

- The simulation and experimental results of obstacle avoidance algorithm are shown in obstacle avoidance using 2 static obstacles, obstacle avoidance using moving obstacle with transversal direction and obstacle avoidance using moving obstacle with transversal direction. The simulation and experimental results of obstacle avoidance algorithm show that the AGV can get successfully the right decision to avoid the obstacle. The reaction is fast enough to prevent the collision condition.

The effectiveness of the proposed algorithm is shown through simulation and experimental results. The AGV can follow the desired velocity and orientation reference signals. Furthermore based on the obstacle avoidance algorithm, the AGV is successfully reached the goal position in unknown environment with avoiding the stationary and moving obstacle. So the system can be applicable and implemented in practical.

## **6.2. Future works**

In the real AGV system, there are a lot of kinds unknown and noise which decrease the control performances such as the frequency response and loading sensitivity. To improve the control performance, those parameters can be considered in mathematic modeling and control design.

The sampling time of positioning method based on the laser navigation system is limited. To improve the positioning accuracy,

the laser positioning result can be combined with encoder of each wheel. Combining the measurement result and output prediction using Kalman filter also can improved the positioning accuracy of AGV.

The proposed obstacle avoidance algorithm in this thesis is only considered about stationary obstacle and single moving obstacle. Therefore, the multi moving obstacle avoidance algorithm should be developed to apply the AGV in real environment.



## References

- [1]. S. Anil Kumar, “*Production and Operation Management*”, New Age International Ltd., New Delhi, 2006.
- [2]. R. K. Duhan, “*The Study of Production Output of Flexible Manufacturing Cells with AGV and Simulation with SIMAN Language*”, International Journal of Engineering Sciences IJMRS, Vol. 1 (2), pp.44-47, 2012.
- [3]. D. Lecking, “*Variable Pallet Pick-Up for Automatic Guided Vehicles in Industrial Environments*”, Proceedings of Emerging Technologies and Factory Automation ETFA '06, pp. 1169 – 1174, 2006.
- [4]. D. Herrero-Pérez and H. Martínez-Barberá, “*Modeling Distributed Transportation Systems Composed of Flexible Automated Guided Vehicles in Flexible Manufacturing Systems*”, Journal of IEEE Transactions on Industrial Informatics, Vol. 6 (2), pp. 116-180, 2010.
- [5]. J. F. Engleberger, “*Health-care Robotics Goes Commercial: The HelpMate' Experience*”, Journal of Robotica, Vol. 11, pp. 517-523, 1993.
- [6]. B. Graf, M. Hans, and R. D. Schraft, “*Care-O-bot II—Development of a Next Generation Robotic Home Assistant*”, Journal of Autonomous robots, Vol. 16 (2), pp.193-205, 2004.
- [7]. F. Carreira et al., “*i-Merc: A Mobile Robot to Deliver Meals Inside Health Services*”, Proceedings of the 2006 IEEE International Conference on Cybernetics & Intelligence Systems & Robotics, Automation & Mechatronics, pp.1-8, 2006.

- [8]. A. G. Ozkil et al., “*Design of a Robotic Automation System for Transportation of Goods in Hospitals*”, Proceedings of International Symposium on Computational Intelligence in Robotics and Automation, 2007. CIRA 2007, pp. 392-397, 2007.
- [9]. G. Belforte, “*Robot Design and Testing for Greenhouse Applications*”, Journal of Biosystems Engineering, Vol. 95 (3), pp. 309–321, 2006.
- [10]. D. L. Peterson, “*A System Approach to Robotic Bulk Harvesting of Apples*”, Journal of American Society of Agricultural Engineers, Vol. 42 (4), pp. 871-876, 1999.
- [11]. T. Chateau, et al, “*Automatic Guidance of Agricultural Vehicles using a Laser Sensor*”, Journal of Computers and Electronics in Agriculture, Vol. 28, pp. 243–257, 2000.
- [12]. H. Rashidi, E. P. K. Tsang, “*Novel Constraints Satisfaction Models for Optimization Problems in Container Terminals*”, Journal of Applied Mathematical Modeling, 2012.
- [13]. “*American Society of Mechanical Engineers’ Safety Standard for Guided Industrial Vehicle and Automated Functions of Manned Industrial Vehicle*”. Technical Report ASME B56.5, 1993.
- [14]. J. W. Mroszczyk, “*Safety Practices for Automated Guided Vehicles (AGV)*”, American Society of Safety Engineers, USA, 2010.
- [15]. L. Armesto, “*Automation of Industrial Vehicles: A Vision-based Line Tracking Application*”, Proceedings of IEEE Conference on Emerging Technologies & Factory Automation 2009, pp. 1-7, 2009.

- [16]. C. R. Kelber, “*Non-Linear Steering Control Strategy for an Optical Stripe Tracker*”, Proceedings of 7th International Workshop on Advanced Motion Control 2002, pp. 546-550, 2002.
- [17]. P. T. Doan, “*Control of Automated Guided Vehicle for Path Following Using Camera Sensor*”, Master Thesis Department of Interdisciplinary Program of Mechatronics Engineering, Pukyong National University, 2011.
- [18]. C. Chen, et al, ”*Application of Automated Guided Vehicle (AGV) Based on Inductive Guidance for Newsprint Rolls Transportation System*”, Journal of Donghua University Vo1. 21 (2), pp. 88-92, 2004.
- [19]. T. Fujimoto, “*Semi-guided Navigation of AGV Through Iterative Learning*”, Proceedings of IEEE/RSJ International Conference on Intelligent Robots and Systems 2001, pp. 968-973, 2001.
- [20]. S. Y. Lee and H. W. Yang, “*Navigation of Automated Guided Vehicles using Magnet Spot Guidance Method*”, Journal of Robotics and Computer-Integrated Manufacturing, Vol. 28 (2), pp. 425-436, 2012.
- [21]. S. C. Yuan, “*Robust Type-2 Fuzzy Control of an Automatic Guided Vehicle for Wall-Following*”, Proceedings of International Conference of Soft Computing and Pattern Recognition, 2009. SOCPAR '09, pp. 172-177, 2009.
- [22]. H. Golnabi, “*Role of Laser Sensor Systems in Automation and Flexible Manufacturing*”, Journal of Robotics and Computer Integrated Manufacturing, Vol. 19, pp. 201–210, 2003.

- [23]. E. K. Jung, et al, "*Implementation of Laser Navigation System using Particle Filter*", Proceedings of 11th International Conference on Control, Automation and Systems, pp. 1636 - 1638, 2011.
- [24]. E. K. Jung, et al, "*Localization for Fork-lift AGV Using Extended Kalman Filter*", Journal of Advances in Mechanical Engineering, Vol. 1 (1), pp. 15-20, 2011.
- [25]. J. M. Kim, et al, "*Positioning Accuracy Improvement of Laser Navigation Using Unscented Kalman Filter*", Journal of Advances in Intelligent Systems and Computing, Vol. 193, pp. 807-816, 2012.
- [26]. P. M. Vaz, "*Docking of a Mobile Platform based on Infrared Sensors*", Proceedings of the IEEE International Symposium on Industrial Electronics, 1997. ISIE '97, Vol. 2, pp. 735 – 740, 1997.
- [27]. F. Tong, "*A High Precision Ultrasonic Docking System used for Automatic Guided Vehicle*", Journal of Sensors and Actuators A: Physical, Vol. 118, pp. 183-189, 2005.
- [28]. R. V. Bostelman, "*Safety Standard Advancement Toward Mobile Robot Use Near Humans*", Proceedings of 4<sup>th</sup> International Conference on Safety of Industrial Automated System, RIA SIAS 2005, pp. 1-8, 2005.
- [29]. G. Spampinato, "*Stereo Vision based Navigation for Automated Vehicles in Industry*", Proceedings of IEEE Conference on Emerging Technologies & Factory Automation, 2009, ETFA 2009, pp. 1-4, 2009.

- [30]. M. Seelinger, “*Automatic Visual Guidance of a Forklift Engaging a Pallet*”, Journal of Robotics and Autonomous Systems, Vol. 54 (12), pp. 1026–1038, 2006.
- [31]. M. Yahyei, “*Increasing the Flexibility and Intelligence of Material Handling through the Factory by Integrated Fuzzy Logic Controller with Programmable Logic Controller*”. Proceedings of 14<sup>th</sup> IEEE International Conference on Fuzzy Systems, 2005. FUZZ '05, pp. 408-413, 2005.
- [32]. N. Kimura, “*Detecting Other Robots from Range Data for Robust Self-Localization of Autonomous Mobile Robots*”, Proceedings of 4<sup>th</sup> International Conference on Intelligent and Advanced Systems (ICIAS2012), pp. 654-658, 2012.
- [33]. X. M. Tao, “*Local Obstacle Avoidance Planning of Logistics System AGV Based Vector Field*”, Proceedings of International Conference on Management Science and Industrial Engineering 2011 (MSIE), pp. 1256-1259, 2011.
- [34]. L. Tang, “*A Novel Potential Field Method for obstacle Avoidance and Path Planning of Mobile Robot*”, Proceedings of 3<sup>rd</sup> IEEE International Conference on Computer Science and Information Technology 2010 (ICCSIT), Vol. 9, pp. 633-637, 2010.
- [35]. A. Elfes, “*Sonar-based Real-world Mapping and Navigation*,” IEEE Journal of Robotics and Automation, Vol. 3, pp. 249-265. 1987.
- [36]. R. X. Jiang, “*A Robot Collision Avoidance Scheme based on the Moving Obstacle Motion Prediction*”, Proceedings of ISECS International Colloquium on Computing,

- Communication, Control, and Management 2008, pp. 341-345, 2008.
- [37]. F. He, Z. Du, “*Laser Range Finder Based Moving Object Tracking and Avoidance in Dynamic Environment*”, Proceedings of IEEE International Conference on Information and Automation 2010 (ICIA), pp. 2357-2362, 2010.
- [38]. J. Borenstein, Y. Koren, “*Obstacle Avoidance with Ultrasonic Sensors*”, Journal of Robotic and Automation, Vol. 4 (1988), pp. 213-218.
- [39]. R. Siegwart, “*Introduction to Autonomous Mobile Robots*”, The Massachusetts Institute of Technology Press, London, England, 2004.
- [40]. H. H. Lin, C. C. Tsai, “*Laser Pose Estimation and Tracking using Fuzzy Extended Information Filtering for an Autonomous Mobile Robot*”, Journal of Intelligent Robotic system, Vol. 53 (2), pp 119-143, 2008.
- [41]. T. Y. Abdalla, A.A. Abdulkarem, “*PSO-based Optimum Design of PID Controller for Mobile Robot Trajectory Tracking*”, International Journal of Computer Applications, Vol. 47 (23), pp. 30-35, 2012.
- [42]. A. Filipescu, “*Trajectory-tracking and Discrete-time Sliding-mode Control of Wheeled Mobile Robots*”, IEEE International Conference on Information and Automation 2011 (ICIA), pp. 27-32, 2011.
- [43]. F. Pourboghrat, “*Exponential stabilization of nonholonomic mobile robots*”, Journal of Computers and Electrical Engineering, Vol. 28, pp. 349-359, 2002.

- [44]. J. G. Kim, et al, "*Development of Navigation Control Algorithm for AGV Using D\* search Algorithm*", Proceeding of 1<sup>st</sup> International Joint Conference on Advanced Engineering, pp. 103-108, 2012.
- [45]. A. K. Tran, "*A study on an Obstacle Avoidance Mobile Robot Using a Ceiling-mounted Camera System*", Master Thesis Department of Interdisciplinary Program of Mechatronics Engineering, Pukyong National University, 2004.
- [46]. H. Giang, et al, "*Path Tracking Controller of Quadruped Robot for Obstacle Avoidance Using Potential Functions Method*", Proceeding of 1<sup>st</sup> International Joint Conference on Advanced Engineering, pp. 122-128, 2012.



## Publications and Conferences

1. Pandu Sandi Pratama, Ngo Manh Dung, Soon Sil Park, Hak Kyeong Kim, Gi Sig Byun and Sang Bong Kim, “*Voltage Control and Current Control for a Digital Gas Metal Arc Welding System Using P Control Method and Fuzzy-Sliding Mode Method*”, Proceeding of The 2011 International Symposium on Mechatronics and Robotics, pp. 185-192, 2011.
2. Pandu Sandi Pratama, Tan-Tung Phan, Hak Kyeong Kim, and Sang Bong Kim, “*A Hybrid Controller Design for Keeping Constant Voltage and Current of a Gas Metal Arc Welding System*”, Proceeding of the 2011 International Symposium on Advance Engineering, pp. 121-126, 2011.
3. Phuc Thinh Doan, Pandu Sandi Pratama, Suk Yoel Kim, Hak Kyeong Kim, “*Developmet of Digital Gas Metel Arc Welding System and Welding Current Control Using Self-tuning Fuzzy PID*”, Journal of The Korean Society of Ocean Engineering (KSOE), Vol. 6, pp. 1-8, 2012.
4. Pandu Sandi Pratama, Sang Kwun Jeong, Soon Sil Park, Sang Bong Kim, “*Moving Object Tracking and Avoidance Algorithm for Differential Driving AGV Based on Laser Measurement Technology*”, Proceeding of 1<sup>st</sup> International Joint Conference on Advanced Engineering, pp. 78-83, 2012.
5. Chetanraj Patil, Pandu Sandi Pratama, Hak Kyeong Kim, Sang Bong Kim, “*Control of Two Wheeled Inverted Pendulum, using Kalman Filter and Backstepping Controller*”, Proceeding of

2012 International Symposium on advanced Mechanical and Power Engineering, pp. 34, 2012.

6. Pandu Sandi Pratama, Sang Kwun Jeong, Soon Sil Park, Sang Bong Kim, “*Moving Object Tracking and Avoidance Algorithm for Differential Driving AGV Based on Laser Measurement Technology*”, International Journal of Science and Engineering, Vol. 4(1), pp. 11-15, 2013.



# Appendix A

## Line-line intersection

Two lines  $L_1$  and  $L_2$  in 2 dimensional space are intersected. Line  $L_1$  is defined by two distinct points  $(x_1, y_1)$  and  $(x_2, y_2)$ , and line  $L_2$  is defined by two distinct points  $(x_3, y_3)$  and  $(x_4, y_4)$  as shown in Fig. A.1

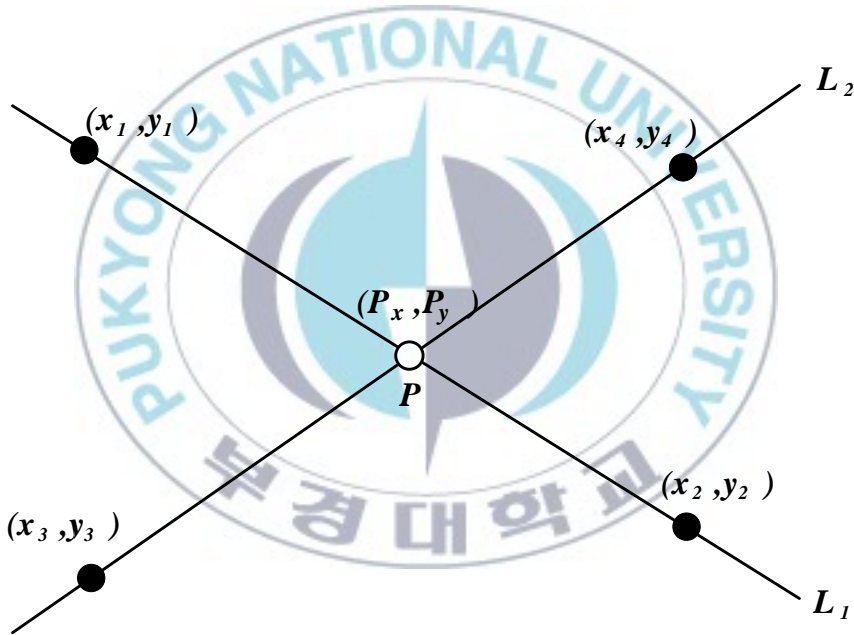


Fig. A.1 The intersection line

The intersected point  $P$  of line  $L_1$  and  $L_2$  can be defined using determinants.

$$P_x = \frac{\begin{vmatrix} x_1 & y_1 & x_1 & 1 \\ x_2 & y_2 & x_2 & 1 \\ x_3 & y_3 & x_3 & 1 \\ x_4 & y_4 & x_4 & 1 \end{vmatrix}}{\begin{vmatrix} x_1 & 1 & y_1 & 1 \\ x_2 & 1 & y_2 & 1 \\ x_3 & 1 & y_3 & 1 \\ x_4 & 1 & y_4 & 1 \end{vmatrix}} \quad P_y = \frac{\begin{vmatrix} x_1 & y_1 & y_1 & 1 \\ x_2 & y_2 & y_2 & 1 \\ x_3 & y_3 & y_3 & 1 \\ x_4 & y_4 & y_4 & 1 \end{vmatrix}}{\begin{vmatrix} x_1 & 1 & y_1 & 1 \\ x_2 & 1 & y_2 & 1 \\ x_3 & 1 & y_3 & 1 \\ x_4 & 1 & y_4 & 1 \end{vmatrix}} \quad (\text{A.1})$$

The determinants can be written out as:

$$(P_x, P_y) = \left( \frac{(x_1 y_2 - y_1 x_2)(x_3 - x_4) - (x_1 - x_2)(x_3 y_4 - y_3 x_4),}{(x_1 - x_2)(y_3 - y_4) - (y_1 - y_2)(x_3 - x_4)}, \frac{(x_1 y_2 - y_1 x_2)(y_3 - y_4) - (y_1 - y_2)(x_3 y_4 - y_3 x_4)}{(x_1 - x_2)(y_3 - y_4) - (y_1 - y_2)(x_3 - x_4)} \right) \quad (\text{A.2})$$

When the two lines are parallel or coincident, the denominator term is zero as follows:

$$(x_1 - x_2)(y_3 - y_4) - (y_1 - y_2)(x_3 - x_4) = 0 \text{ if the lines are parallel}$$